



Proteomic profiling of VCP substrates links VCP to K6-linked ubiquitylation and c-Myc function

Jan B Heidelberg¹, Andrea Voigt¹, Marina E Borisova¹, Giuseppe Petrosino¹, Stefanie Ruf¹, Sebastian A Wagner^{2,*}  & Petra Belli^{1,**} 

Abstract

Valosin-containing protein (VCP) is an evolutionarily conserved ubiquitin-dependent ATPase that mediates the degradation of proteins through the ubiquitin–proteasome pathway. Despite the central role of VCP in the regulation of protein homeostasis, identity and nature of its cellular substrates remain poorly defined. Here, we combined chemical inhibition of VCP and quantitative ubiquitin remnant profiling to assess the effect of VCP inhibition on the ubiquitin-modified proteome and to probe the substrate spectrum of VCP in human cells. We demonstrate that inhibition of VCP perturbs cellular ubiquitylation and increases ubiquitylation of a different subset of proteins compared to proteasome inhibition. VCP inhibition globally upregulates K6-linked ubiquitylation that is dependent on the HECT-type ubiquitin E3 ligase HUWE1. We report ~450 putative VCP substrates, many of which function in nuclear processes, including gene expression, DNA repair and cell cycle. Moreover, we identify that VCP regulates the level and activity of the transcription factor c-Myc.

Keywords c-Myc; HUWE1; K6-linked ubiquitylation; ubiquitin remnant profiling; VCP

Subject Categories Methods & Resources; Post-translational Modifications, Proteolysis & Proteomics

DOI 10.15252/embr.201744754 | Received 3 July 2017 | Revised 17 January 2018 | Accepted 26 January 2018 | Published online 21 February 2018

EMBO Reports (2018) 19: e44754

Introduction

Regulated protein degradation through the ubiquitin–proteasome and autophagy–lysosome pathway plays essential roles in the maintenance of cellular homeostasis [1]. Functional dysregulation of these degradation mechanisms is associated with the development of neurodegenerative diseases and cancer [2–6]. Valosin-containing protein (VCP, also known as p97) is an evolutionarily conserved chaperone-like AAA ATPase that structurally remodels

ubiquitylated substrates prior to their degradation by the proteasome [7–10]. VCP executes its cellular functions in conjunction with different adaptor proteins that contain ubiquitin-binding domains and hence mediate the interaction with substrates. The majority of known VCP adaptors harbor ubiquitin-X (UBX) or UBX-like domains that bind to the N-terminus of VCP [11,12]. VCP has been extensively studied in the context of the endoplasmic reticulum-associated degradation (ERAD), where it is essential for the extraction of misfolded proteins from the ER membrane [13,14]. In addition, VCP is involved in the degradation of protein aggregates, stress granules, and organelles through the autophagy–lysosome pathway [15–18]. More recent studies showed that VCP can also remodel proteins in other cellular compartments, including nucleus and outer mitochondrial membrane, and that VCP-mediated remodeling is not necessarily associated with protein degradation [19–22]. However, despite the essential role of VCP in the remodeling and degradation of proteins, the scope and nature of its substrates in human cells remain poorly understood.

Inhibition of the ubiquitin–proteasome system (UPS) by proteasome inhibitors is effective in the treatment of multiple myeloma that has been shown to display high levels of proteotoxic stress [23,24]. Targeting other components of the UPS, including VCP, emerged as a promising therapeutic strategy for the treatment of cancer [25]. A recent study reported the synthesis and characterization of the potent, orally bioavailable VCP inhibitor CB-5083 that is currently in clinical trials for the treatment of refractory multiple myeloma and advanced solid tumors [26].

Previous studies employed affinity purification of VCP adaptors or size exclusion chromatography after VCP inhibition combined with quantitative mass spectrometry (MS) for systematic analysis of VCP substrates in human cells [27,28]. Recently, methods for mapping of endogenous ubiquitylation sites based on the enrichment of ubiquitin remnant (di-glycine-modified) peptides followed by identification using MS were introduced [29–31]. Functional inhibition of VCP leads to increased ubiquitylation of substrate proteins, which is a consequence of their inability to undergo proteasomal degradation or merely extraction from cellular structures or larger protein complexes [26,32,33].

1 Institute of Molecular Biology (IMB), Mainz, Germany

2 Department of Medicine, Hematology/Oncology, Goethe University School of Medicine, Frankfurt, Germany

*Corresponding author. Tel: +49 69 63016358; E-mail: swagner@med.uni-frankfurt.de

**Corresponding author. Tel: +49 6131 3921590; E-mail: p.belli@imb-mainz.de

Therefore, to reveal the substrate spectrum of VCP in human cells, we employed quantitative MS based on stable isotope labeling with amino acids in cell culture (SILAC) and ubiquitin remnant profiling for proteome-wide analysis of ubiquitylation sites after chemical inhibition of VCP. We demonstrate that inhibition of VCP globally perturbs cellular ubiquitylation patterns and results in increased ubiquitylation of a different subset of proteins compared to proteasome inhibition. We show that VCP inhibition increases the abundance of K6-linked ubiquitylation that is dependent on the HECT-type ubiquitin ligase HUWE1. We further used a K6-linked ubiquitin-specific affimer to identify proteins modified with K6-linked ubiquitylation. Our data uncover ~450 putative VCP substrates, many of which are present in the nucleus, and function in gene expression, DNA repair and cell cycle regulation. Moreover, we identify the transcription factor c-Myc as a novel chromatin-associated substrate of VCP and demonstrate that VCP regulates the level and activity of c-Myc.

Results

VCP inhibition globally perturbs cellular ubiquitylation patterns

To compare the changes in cellular ubiquitylation after VCP and proteasome inhibition, human osteosarcoma (U2OS) cells were treated with the allosteric VCP inhibitor NMS-873, the competitive VCP inhibitor CB-5083, or the proteasome inhibitor MG132 [26,33]. Western blot analysis of protein ubiquitylation in total cell lysates showed that treatment of cells with VCP inhibitors substantially increased the abundance of ubiquitylated protein species as previously reported [26,33] (Fig EV1A and B). An even greater increase in protein ubiquitylation was observed in cells treated with the proteasome inhibitor, showing that VCP inhibition selectively increases the ubiquitylation of a smaller set of proteins (Fig 1A). Increasing concentrations of VCP inhibitor did not further increase the amount of ubiquitylation, indicating that the observed effect on protein ubiquitylation is selective and not caused by incomplete inhibition of VCP (Fig EV1A).

Next, we employed MS-based proteomics to assess the effect of chemical inhibition of VCP on the ubiquitin-modified proteome in a site-specific manner. A side-to-side comparison of protein ubiquitylation after VCP and proteasome inhibition was used to differentiate between proteasome-dependent and independent effects. We employed SILAC to quantify ubiquitylation site abundance in the different experimental conditions: “light” labeled cells were mock-treated, “medium” labeled cells were treated with the proteasome inhibitor MG132, and “heavy” labeled cells with the VCP inhibitor NMS-873 or CB-5083 (Fig 1B). In addition to the ubiquitin-modified proteome, we also quantified the changes in protein abundance in the same experiment. Using this strategy, we quantified 7,464 endogenous di-glycine-modified sites after treatment of cells with NMS-873, of which 63% and 40% were quantified in two and three independent replicate experiments, respectively (Fig 1C, Dataset EV1). Note that di-glycine-modified peptides can also result from tryptic digestion of NEDD8 and ISG15-modified proteins; however, due to the low cellular occurrence of these modifications, it is likely that a large majority of the quantified di-glycine-modified peptides originate from ubiquitylated proteins. The replicate experiments showed a high quantitative reproducibility ($\rho = 0.82-0.9$; Figs 1D and EV1C). VCP inhibition globally perturbed cellular ubiquitylation patterns, but resulted in an upregulation of a relatively smaller fraction of sites compared to inhibition of the proteasome (Fig 1E). Inhibition of the proteasome increased the abundance of 45% of all quantified ubiquitylation sites, whereas 16% of sites increased in abundance after chemical inhibition of VCP (Fig 1E). Inhibition of VCP using different inhibitors, NMS-873 and CB-5083, showed similar effects on ubiquitylation site abundance ($\rho = 0.63$, P value = 0) (Fig EV1D, Dataset EV2). Despite the dramatic effects on protein ubiquitylation, cellular protein levels were only slightly affected by inhibition of VCP or the proteasome (Fig 1F). We found that the abundance of 25 proteins increased more than twofold after VCP inhibition and that the majority of these proteins is involved in the unfolded protein response as previously reported [26,33] (Fig EV1E).

Figure 1. VCP inhibition globally perturbs cellular ubiquitylation.

- VCP inhibition increases the cellular levels of ubiquitylated protein species. Total cell lysates from mock-treated U2OS cells, cells treated with the proteasome inhibitor MG132 (10 μ M, 6 h), or the VCP inhibitor NMS-873 (5 μ M, 6 h) were separated by SDS-PAGE. Proteins were detected by indicated antibodies.
- Schematic representation of the experimental strategy for quantitative analysis of ubiquitylation sites and proteins after chemical inhibition of VCP. “Light” labeled U2OS cells served as control, whereas “medium” and “heavy” labeled cells were treated with MG132 (10 μ M, 6 h) and NMS-873 (5 μ M, 6 h) or CB-5083 (0.5 μ M, 6 h), respectively. Cells were lysed, and equal amounts of proteins extracted from three differentially labeled cell populations were pooled and digested in solution with trypsin. Ubiquitin remnant peptides were enriched using di-glycine-lysine-specific antibodies and fractionated by micro-SCX. For proteome analysis, proteins were separated by SDS-PAGE and digested in-gel using trypsin. Peptide fractions were analyzed by LC-MS/MS, and the raw data were processed using MaxQuant software.
- The bar graph shows the number of sites quantified in 1, 2, 3, or 4 ubiquitin remnant profiling replicate experiments. The line indicates the cumulative fraction of sites quantified in at least 1, 2, 3, or 4 replicate experiments.
- Quantitative reproducibility between the replicate experiments. The heat map shows the Spearman’s rank correlation coefficient that was calculated to determine the experimental reproducibility of ubiquitylation sites quantified after VCP inhibition.
- The cumulative density plot shows the distribution of logarithmized SILAC ratios of quantified di-glycine-modified (e.g., ubiquitylated) peptides in ubiquitin remnant profiling experiments after VCP or proteasome inhibition. VCP inhibition increases the abundance of 16%, whereas proteasome inhibition 45% of quantified ubiquitylation sites.
- Inhibition of VCP and proteasome has a minor effect on protein levels. The density plot shows the distribution of logarithmized SILAC ratios of quantified protein groups after VCP or proteasome inhibition.
- Quantification of the free ubiquitin pool in cells treated with VCP inhibitor NMS-873 or proteasome inhibitor MG132. Cells were treated with MG132 (10 μ M) or NMS-873 (5 μ M) for different time points, and the free ubiquitin levels were quantified. The bar plots show the mean and SD calculated from three replicate experiments. The values were normalized to the DMSO-treated control. Antibody against ubiquitin (P4D1) was used to detect free ubiquitin using Western blotting.

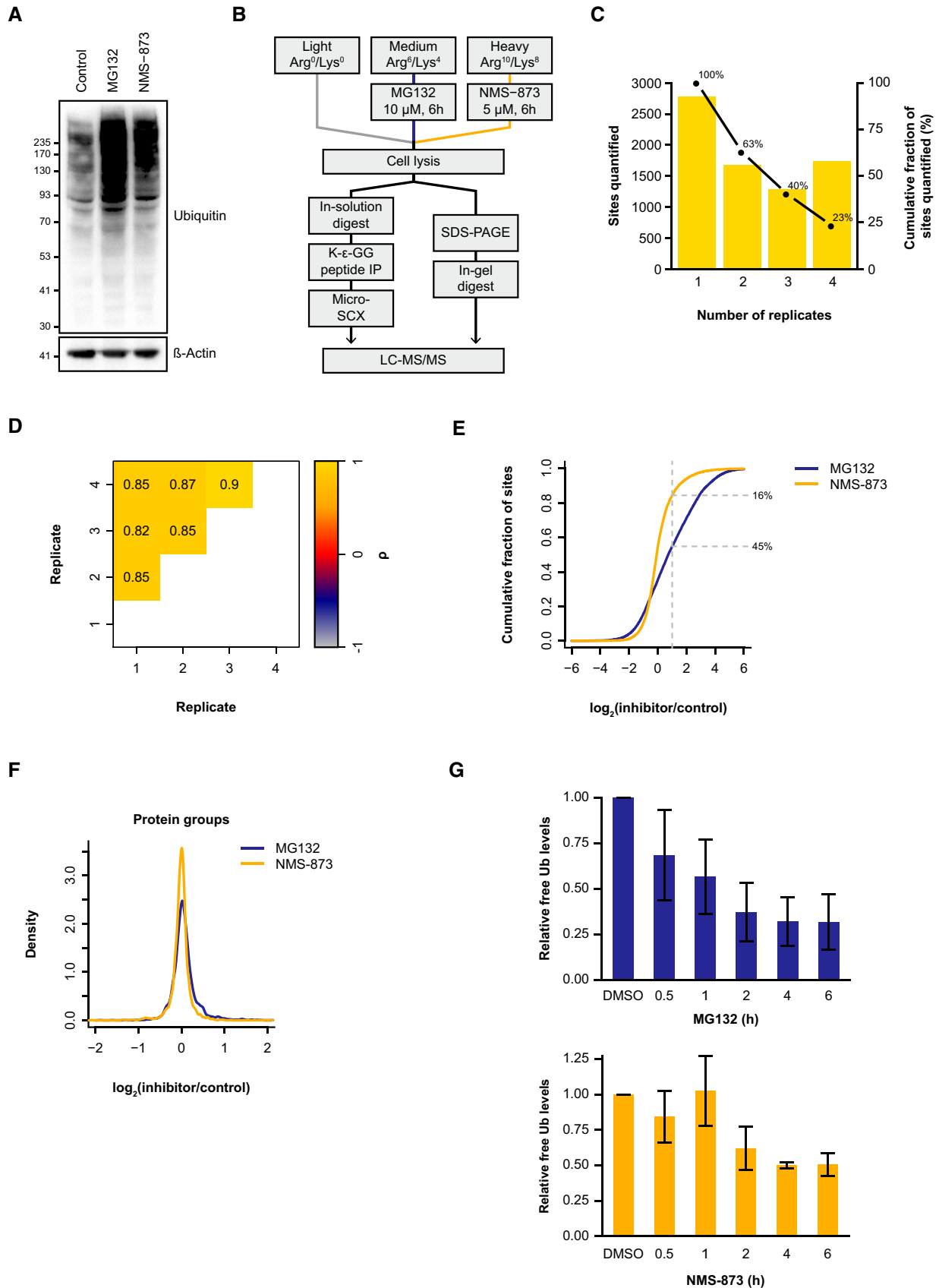


Figure 1.

All core histones and ribosomal proteins that are known to be modified by non-degradative, regulatory ubiquitylation showed decreased ubiquitylation after VCP inhibition, indicative of the cellular ubiquitin pool depletion that was shown to occur as consequence of proteasome inhibition (Fig EV1F) [29,31,34–36]. Indeed, relative quantification of the free ubiquitin pool revealed a twofold reduction in free ubiquitin levels after 4-h treatment of cells with NMS-873 (Fig 1G).

VCP inhibition increases the cellular abundance of K6-linked ubiquitylation

VCP has been shown to target proteins modified with homotypic K48-linked and heterotypic K11/K48-branched ubiquitin chains for proteasomal degradation [7–9,37–42]. However, it remains unclear whether other types of ubiquitin chains can serve as signal for protein remodeling or degradation by VCP. To gain insights into the ubiquitin signals that are important for VCP functions, we investigated the cellular abundance of all seven internal ubiquitin linkage types. Based on the SILAC ratio of the ubiquitin linkage-specific peptides quantified in ubiquitin remnant profiling experiments, we determined the relative changes in ubiquitin linkage type in cells after VCP or proteasome inhibition. Notably, the ubiquitin remnant peptide resulting from tryptic digestion of K6-linked ubiquitin showed a significant increase in abundance after VCP inhibition but not after proteasome inhibition (4.6-fold after 6-h treatment), pointing to a possible role of this atypically linked ubiquitin in VCP functions (Fig 2A and B). K48-linked ubiquitylation increased in abundance to a similar extent after both treatments and the abundance of K63-linked ubiquitylation did not significantly change (Fig 2A). In agreement with previous studies that reported the role for K11-linked ubiquitylation and K11/K48-branched ubiquitin chains in VCP functions [37–39,41–43], K11-linked ubiquitylation increased in abundance after VCP inhibition (Fig 2A). We observed that K27-linked ubiquitylation specifically decreased in abundance after treatment of cells with the VCP inhibitor (Fig 2A). To exclude possible indirect effects of the ubiquitin pool depletion on the abundance of different ubiquitin linkages, we performed a time course experiment that revealed an increase in K6-linked ubiquitylation already 30 min after treatment of cells with the VCP inhibitor (Fig 2C). At this early time point, we did not observe any effect of

VCP inhibition on free ubiquitin levels (Fig 1G). Importantly, the increase in the cellular abundance of K6-linked ubiquitin was also observed after transient knockdown of VCP (Fig EV2A). We could validate the increase of K6-linked ubiquitylated protein species using a K6-linked ubiquitin-specific affimer and Western blotting with an ubiquitin-specific antibody (Fig EV2B).

To date, only the ubiquitin ligase parkin that plays a role in mitophagy has been unambiguously demonstrated to assemble K6-linked ubiquitylation *in vivo* [44–46], leaving the scope and function of this atypical ubiquitylation largely unexplored. Therefore, we performed a pull down of ubiquitylated proteins using the K6-linked ubiquitin-specific affimer [47] to identify proteins that are modified with K6-linked ubiquitylation after inhibition of VCP by quantitative MS (Dataset EV3). From four replicate experiments, we identified 83 proteins that were consistently enriched in the K6-linked ubiquitin-specific affimer pull downs and are therefore likely modified with K6-linked ubiquitin (Fig EV2C). Because these pull downs could not be performed under denaturing conditions, it is possible that some of these proteins tightly bind to K6-linked ubiquitylated proteins. Interestingly, the majority of the identified proteins is involved in receptor endocytosis, cell cycle, ERAD pathway, or proteasomal degradation, pointing to a functional role of K6-linked ubiquitylation and VCP in these cellular processes (Fig 2D). In addition, we found a group of proteins that is not engaged in any functional associations (Fig 2D). Considering that K11- and K48-linked ubiquitylation also increases in abundance after VCP inhibition, it is likely that some of these proteins are modified with heterotypic (mixed or branched) ubiquitin chains consisting of K6/K11/K48 linkages. Comparison of the results of the K6-linked ubiquitin-specific pull downs with ubiquitin remnant profiling experiments showed that proteins identified in the K6-linked ubiquitin-specific pull downs are indeed in average more ubiquitylated after VCP inhibition but not after proteasome inhibition (Fig EV2D). We employed the previously described ubiquitin replacement strategy [48] to confirm the presence of K6-linked ubiquitylation on ARL2, DCAF7, DNAJB2, HGS, and STAM2 (Fig EV2E).

We also identified several ubiquitin ligases in the K6-linked ubiquitin-specific pull downs, among which the HECT-type E3 ligase HUWE1 was most strongly enriched (Fig 2D, Dataset EV3). To test whether HUWE1 might be responsible for assembling K6-linked ubiquitylation that accumulates in cells after VCP inhibition, we

Figure 2. VCP inhibition increases the cellular abundance of K6-linked ubiquitylation.

- Quantification of ubiquitin linkage-specific peptides after proteasome or VCP inhibition. The bar plot shows the mean and SD of logarithmized SILAC ratios VCP or proteasome inhibitor/control of ubiquitin linkage-specific peptides from four replicates. The table indicates the mean of the logarithmized SILAC ratios of ubiquitin peptides corresponding to seven ubiquitin linkages quantified in the four ubiquitin remnant profiling experiments after proteasome (MG132, 10 μ M, 6 h) or VCP (NMS-873, 5 μ M, 6 h) inhibition. Non-paired *t*-test was used to calculate the significance levels from four replicate experiments. The peptide resulting from tryptic digestion of K6-linked ubiquitin increases in abundance exclusively after VCP inhibition.
- Mass spectrometric parent ion scan of the peptide MQIFVK(g)TLTGK resulting from tryptic digestion of K6-linked ubiquitin. The SILAC triplet shows the relative abundance and mass to charge (*m/z*) of the peptide in mock-treated cells and cell treated with MG132 or NMS-873. The relative abundance of the peptide increases 4.3-fold after VCP inhibition.
- The line plot shows logarithmized SILAC ratios VCP inhibitor/control of ubiquitin linkage-specific peptides quantified after treatment of cells with NMS-873 for different time points.
- Functional interaction network of proteins enriched in K6-linked ubiquitin-specific pull downs after VCP inhibition using NMS-873 (5 μ M, 6 h). Only proteins that were found to be significantly enriched from four replicate experiments are shown. Ubiquitin was removed from network for clarity. Proteins identified in the pull down that do not form a functional network are indicated on the right. Proteins with ubiquitylation site(s) that decreased at least twofold after knockdown of HUWE1 in ubiquitin remnant profiling experiment are labeled in red. The complete list of quantified proteins can be found in Dataset EV3.
- HUWE1 knockdown decreases the abundance of K6-linked ubiquitin. The bar plot shows logarithmized SILAC ratios HUWE1 knockdown/control of ubiquitin linkage-specific peptides. The complete list of ubiquitylation sites quantified after HUWE1 knockdown can be found in Dataset EV4.

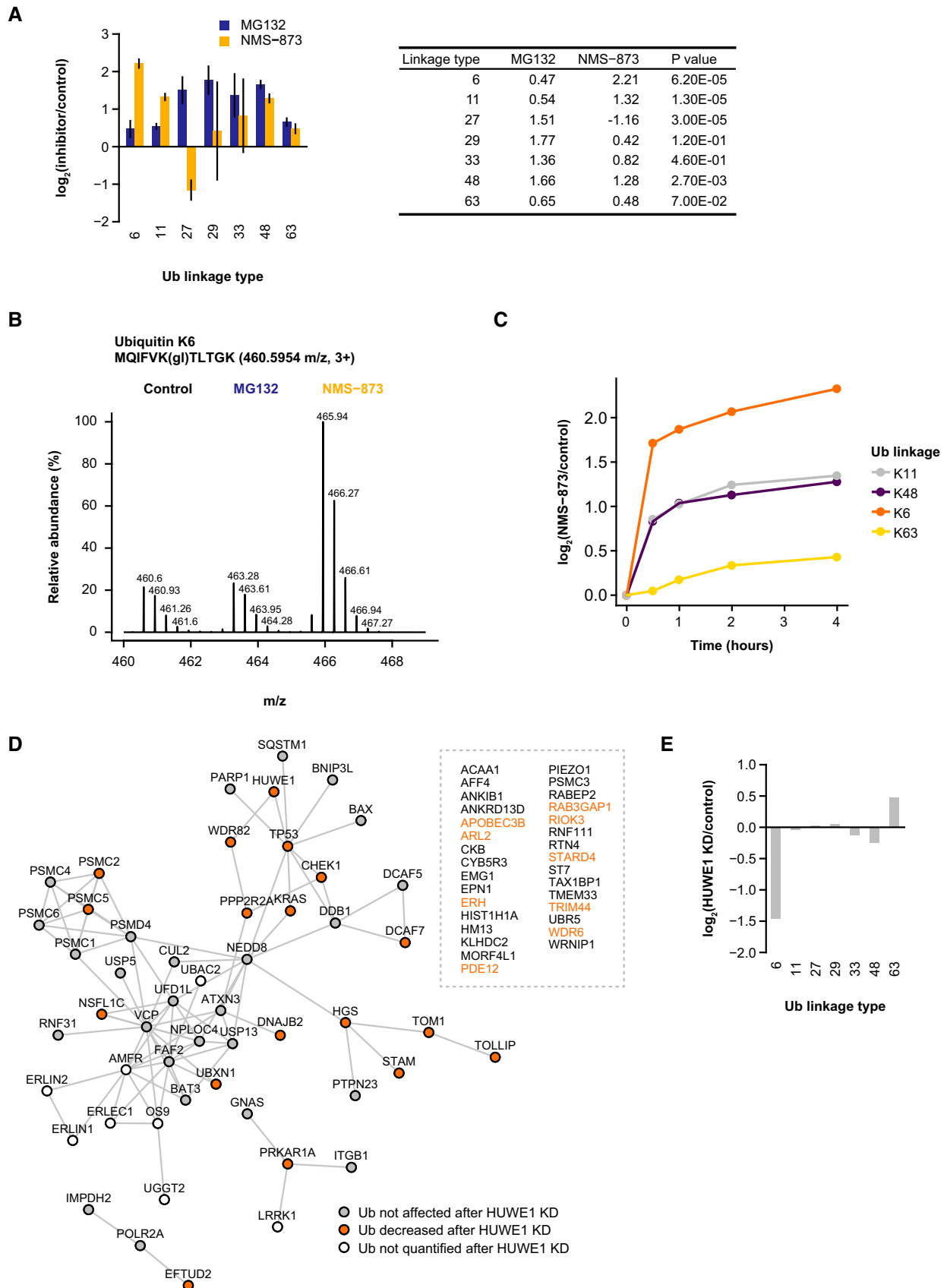


Figure 2.

transiently knocked down HUWE1 expression using siRNA and monitored the abundance of different ubiquitin linkage-specific peptides by ubiquitin remnant profiling (Figs 2E and EV2F). Strikingly, knockdown of HUWE1 resulted in a dramatic decrease of K6-linked ubiquitylation in cells treated with VCP inhibitor, indicating that HUWE1 is responsible for assembling K6-linked ubiquitin on proteins that accumulates after VCP inhibition (Fig 2E). In accordance, ubiquitylation of a large number of proteins identified in the K6-linked ubiquitin-specific pull downs decreased at least twofold after knockdown of HUWE1 (Fig 2D, Dataset EV4). The abundance of K48-linked ubiquitylation also decreased after knockdown of HUWE1, suggesting that HUWE1 assembles heterotypic (mixed or branched) K6/K48-linked ubiquitin chains *in vivo* (Fig 2E, Dataset EV4).

VCP substrates share secondary structure features and many localize to nuclear compartments

The ATPase VCP plays essential roles in remodeling and degradation of cellular proteins; however, identity and properties of its substrates remain largely unknown. To determine significantly regulated ubiquitylation sites after VCP inhibition, we applied a moderated *t*-test (limma algorithm; Figs 3A and EV3A) [49]. This analysis identified 806 significantly upregulated and 636 downregulated sites ($P < 0.01$; Fig 3B, Dataset EV1). Notably, inhibition of the proteasome led to a significant up- and downregulation of a far greater number of ubiquitylation sites compared to VCP inhibition (2,120 and 977, respectively; Fig 3B, Dataset EV1). We considered proteins as putative VCP substrates that showed at least one significantly upregulated ubiquitylation site and no downregulated ubiquitylation sites after VCP inhibition. Based on these criteria, 456 proteins were identified as putative VCP substrates. This group of proteins contained the previously identified VCP substrates XPC, DDB2, RNA pol II, MCM7, and MFN2 supporting the validity of our approach (Dataset EV1) [16,50–56]. It is possible that some of these proteins are not direct substrates of VCP, but that the increase in their ubiquitylation occurs as an indirect consequence of VCP inhibition. Interestingly, we found that one-third of the identified VCP substrates, similarly to proteasome substrates, contain multiple lysine residues that act as ubiquitin acceptor sites (Fig 3C). Next, we investigated whether VCP substrates share common

structural or biochemical properties that can explain why they depend on remodeling by VCP. Secondary structure prediction revealed a significantly higher occurrence of α -helices in VCP substrates compared to non-substrates (Fig 3D). In contrast to α -helices, the frequency of beta-sheet and turn secondary structures as well as the molecular weight did not differ significantly between VCP substrates and non-substrates (Fig 3D and E). Notably, we found that VCP substrates contain less low complexity, disordered regions in their structure than non-substrates or proteasome substrates (Figs 3F and EV3B). VCP substrates are also significantly more hydrophobic in nature than non-substrates (Fig 3G).

In human cells, VCP-dependent protein remodeling was mainly studied in the context of proteasomal degradation of substrate proteins. However, it has been reported that VCP confers proteasome-independent functions in mitosis, where it extracts Aurora B kinase from mitotic chromosomes without subsequent degradation [20,21]. Notably, 119 out of 456 VCP substrates identified in our study displayed increased ubiquitylation exclusively after VCP but not after proteasome inhibition, suggesting that these proteins are subjected to proteasome-independent regulation by VCP (Fig 4A).

Proteins whose ubiquitylation increased in abundance exclusively after VCP inhibition are involved in vesicle-mediated transport and negative regulation of EGFR signaling pathway (Figs 4B and EV4A, Dataset EV5). For instance, components of EGFR signaling pathway and endosome trafficking through the ESCRT pathway such as EPS15, STAM, TOM1, and GRB2 contain ubiquitylation sites that are only upregulated after VCP inhibition ($P < 0.01$; Fig EV4A and B). We also identified STAM and TOM1 in the K6-linked ubiquitin-specific pull downs, suggesting that these proteins are modified by and/or tightly bind to K6-linked ubiquitin chains (Fig 2D).

Proteins whose ubiquitylation increases after VCP and proteasome inhibition are involved in the mitotic nuclear envelope disassembly, cell cycle regulation, gene expression, and DNA repair (Fig 4B–D, Dataset EV5). In addition, proteins localized to membrane compartments including the ER membrane and nuclear pore are overrepresented in this group (Fig 4B and C). Cell cycle regulators including cyclin D1/2, cyclin-dependent kinases 1 and 6, MAD2L1, DDB1/2, MCM7, and GADD45A were also identified as VCP-dependent proteasome substrates (Figs 4C and EV4C). Ubiquitylation of these proteins increased in abundance also after short-term treatment with the VCP inhibitor that does not result in cell

Figure 3. Ubiquitin remnant profiling identifies the cellular substrates of VCP.

- A Identification of significantly upregulated ubiquitylation sites after VCP inhibition from four replicate experiments was done using the limma algorithm. P value < 0.01 corrected for multiple hypothesis testing was used as cutoff to determine upregulated and downregulated ubiquitylation sites after VCP inhibition. Color coding indicates the number of experiments in which the site was quantified. The complete list of regulated ubiquitylation sites and proteins can be found in Dataset EV1.
- B The bar graph shows the number of significantly up-, non-, and downregulated ubiquitylation sites after VCP or proteasome inhibition.
- C VCP substrates are subjected to multisite ubiquitylation. The bar plot shows the fraction of proteins containing 1, 2–3, 4–6, and > 6 upregulated ubiquitylation sites after proteasome or VCP inhibition.
- D Secondary structure properties of VCP substrates. The secondary structure was predicted for identified VCP substrates (proteins with at least one upregulated and no downregulated site after VCP inhibition) and non-substrates (proteins with ubiquitylation sites that were not upregulated after VCP inhibition). VCP substrates display a significantly higher occurrence of α -helices compared to non-substrates, whereas the occurrence of β -sheet and turn structures does not differ significantly.
- E The molecular weight does not differ between VCP substrates and non-substrates.
- F VCP substrates contain less disordered, low complexity regions compared to non-substrate proteins.
- G VCP substrates are significantly more hydrophobic compared to non-substrate proteins. The GRAVY (grand average of hydropathicity) score was calculated for VCP substrates and non-substrates.

Data information: The lower and upper hinges of the box plots represent the first and third quartiles, respectively. The line in the center of the box corresponds to the median of the data range. Significance was estimated using Wilcoxon rank sum test.

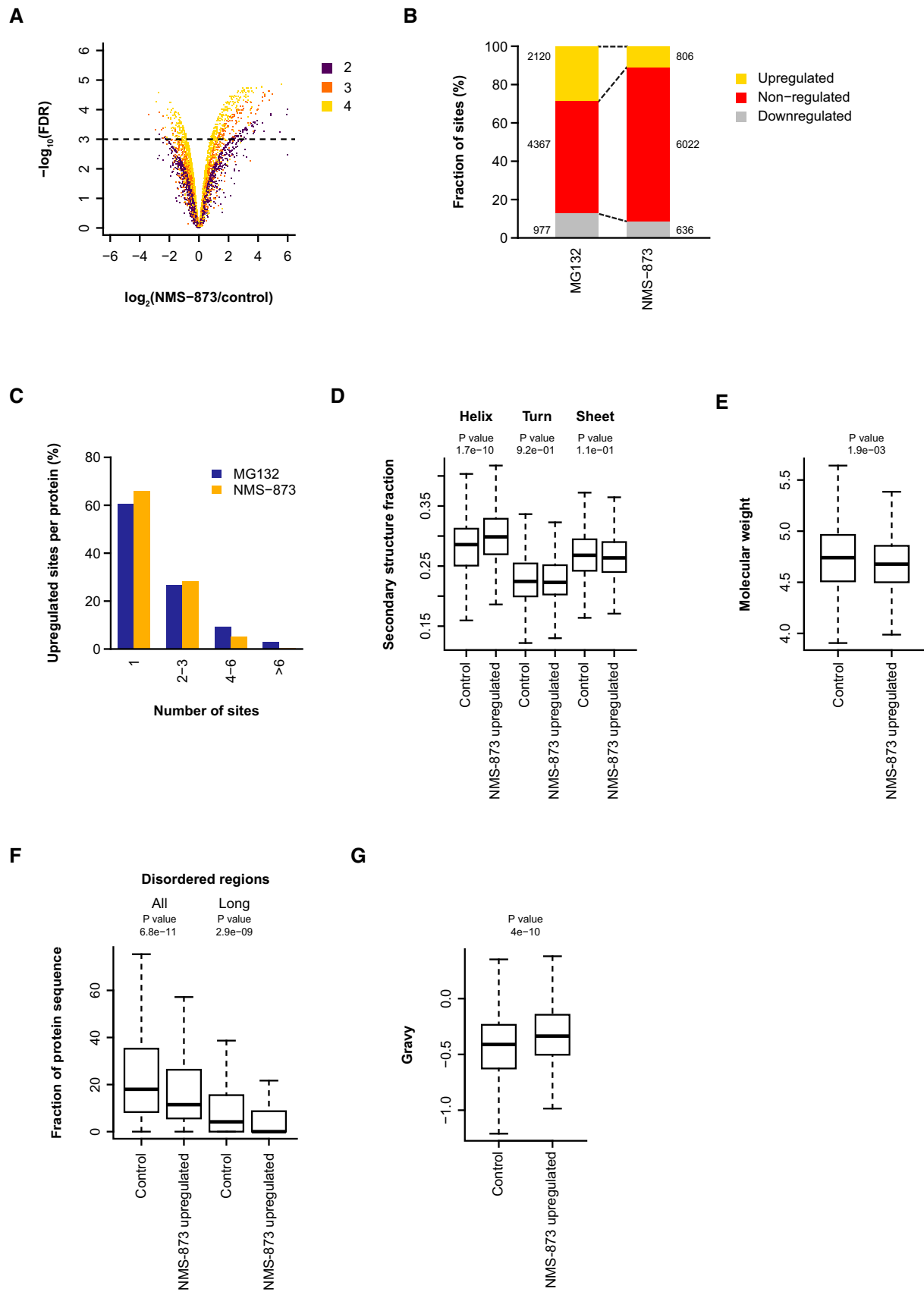


Figure 3.

Figure 4. VCP confers proteasome-dependent and independent functions.

- A The bar plot shows the number of proteins containing upregulated ubiquitylation sites after VCP and proteasome inhibition or exclusively after VCP inhibition. Ubiquitylation of 119 proteins is upregulated exclusively after inhibition of VCP but not the proteasome ($P < 0.01$).
- B Biological processes (BP), cellular compartments (CC), and molecular functions (MF) associated with VCP substrates. The plot shows significantly overrepresented Gene Ontology terms associated with proteasome-dependent and independent VCP substrates compared to non-substrates ($P < 0.01$). Redundant terms were removed for clarity. The complete list of enriched terms can be found in Dataset EV5.
- C Cell cycle regulators and nuclear pore proteins are overrepresented among VCP substrates. Analysis of functional associations among identified VCP substrates involved in the cell cycle regulation and DNA repair. Only interactions with a STRING score above 0.7 are represented in the network. The node size depicts the number of upregulated ubiquitylation sites on the indicated proteins. Proteins with upregulated ubiquitylation sites exclusively after VCP inhibition are shown in orange and proteins with upregulated ubiquitylation sites after VCP and proteasome inhibition are shown in blue. Proteins that contain VCP upregulated and downregulated sites are indicated with the dotted line.
- D Analysis of functional associations among VCP substrates involved in nucleotide-excision repair. The node size depicts the number of upregulated ubiquitylation sites on the indicated proteins. Proteins with upregulated ubiquitylation sites exclusively after VCP inhibition are shown in orange and proteins with upregulated ubiquitylation sites after VCP and proteasome inhibition are shown in blue.
- E The line plot shows logarithmized SILAC ratios VCP inhibitor/control of ubiquitylation sites on different cell cycle regulators quantified after treatment of cells with NMS-873 for different time points.
- F Knockdown of VCP results in G1 and G2/M cell cycle arrest. U2OS cell cycle was analyzed upon knockdown of VCP using two different siRNAs or siRNA pool using flow cytometry.

cycle defects (Fig 4E). In agreement with the finding that many cell cycle regulators are VCP substrates, knockdown of VCP resulted in cell cycle progression defects, which manifested as an arrest of cells in G1 and G2/M phase as it has been previously reported (Fig 4F) [57,58].

VCP regulates the level and function of the transcription factor c-Myc

Level and activity of the transcription factor c-Myc have been shown to be extensively regulated by dynamic ubiquitylation and deubiquitylation that is mediated by a number of ubiquitin ligases and deubiquitylating enzymes [59]. We found that inhibition of VCP and proteasome increases ubiquitylation of c-Myc on lysine 148, suggesting that c-Myc is a substrate of VCP (Figs 5A and EV5A and B). Denaturing pull downs of GFP-tagged c-Myc validated that VCP inhibition results in increased c-Myc ubiquitylation (Fig 5B). To test

whether VCP regulates c-Myc degradation, we chemically inhibited VCP by NMS-873 or CB-5083 and monitored c-Myc levels by Western blotting. The cellular abundance of c-Myc increased ~2-fold after inhibition of VCP supporting that c-Myc is a substrate of VCP-dependent proteasomal degradation (Figs 5C and EV5C–E). VCP inhibition also increased the levels of ectopically expressed tagged c-Myc as expected if VCP regulates c-Myc post-translationally (Fig EV5F). Confocal microscopy of endogenous c-Myc confirmed that the nuclear levels of c-Myc increase after VCP inhibition (Fig EV5G).

To investigate whether c-Myc also interacts with VCP, we pulled down GFP-tagged c-Myc from cellular lysates and identified its interaction partners by SILAC-based quantitative MS. In addition to known interaction partners such as Max [60], VCP was significantly enriched in the c-Myc pull downs (Fig 5D, Dataset EV6). We identified a number of other proteins enriched in c-Myc immunoprecipitates that were previously not reported

Figure 5. Transcription factor c-Myc is a substrate of VCP.

- A c-Myc ubiquitylation on K148 increases after VCP and proteasome inhibition. Mass spectrometric parent ion scan of the peptide LVSEK(g)LASQYQAR corresponding to di-glycine-modified K148 in c-Myc. The SILAC triplet shows the relative abundance and mass to charge (m/z) of the di-glycine-modified peptide in mock-treated cells and cells treated with MG132 or NMS-873.
- B c-Myc ubiquitylation increases after VCP inhibition. GFP-tagged c-Myc was overexpressed in U2OS cells that were either mock-treated or treated with NMS-873 (5 μ M, 6 h). Proteins were extracted from cells, and GFP-tagged c-Myc was enriched using GFP-Trap agarose. Pull downs were washed under denaturing conditions to remove interaction partners and blotted with the ubiquitin antibodies.
- C Cellular levels of c-Myc increase after VCP inhibition. Total cell lysates from U2OS cells treated with increasing concentrations of NMS-873 for 6 h were resolved by SDS–PAGE and subjected to Western blotting. Quantification of the c-Myc Western blot normalized to β -actin 6 h after NMS-873 (5 μ M) treatment is shown. The bar plot shows the mean and SD calculated from four replicate experiments. $**P < 0.01$ (two-tailed, unpaired, equal variance Student's t -test).
- D Identification of c-Myc interaction partners by quantitative MS. c-Myc-GFP and interaction partners were immunoprecipitated from SILAC-labeled U2OS cells using GFP-Trap agarose, and proteins were resolved by SDS–PAGE. After in-gel digestion of proteins using trypsin, peptides were analyzed by LC-MS/MS. Identification of significantly enriched proteins from three replicate experiments was done using the limma algorithm ($P < 0.01$). VCP was specifically pulled down by c-Myc-GFP compared to the control pull down performed from cells expressing GFP only. The complete list of quantified proteins can be found in Dataset EV6.
- E Functional interaction network of identified c-Myc interaction partners. Proteins previously reported to interact with c-Myc in the BioGRID protein–protein interaction database are labeled in yellow.
- F c-Myc interacts with VCP *in vivo*. U2OS cells were co-transfected with c-Myc-GFP and Strep-Flag-VCP, and lysates were subjected to StrepTactin Sepharose pull downs. Enriched proteins were resolved by SDS–PAGE and blotted with the indicated antibodies. Asterisk indicates c-Myc band arising from re-blotting of the membrane.
- G c-Myc interacts with VCP in an ubiquitin-dependent manner. U2OS cells were co-transfected with c-Myc-GFP and Strep-Flag-VCP, and lysates were subjected to StrepTactin Sepharose pull downs. Enriched proteins were treated with the recombinant catalytic domain of USP2, resolved by SDS–PAGE, and blotted with the indicated antibodies. Asterisk indicates c-Myc band arising from re-blotting of the membrane.
- H c-Myc ubiquitylation on K148 decreases after HUWE1 knockdown. Mass spectrometric parent ion scan of the peptide LVSEK(g)LASQYQAR corresponding to di-glycine-modified K148 in c-Myc. The SILAC pair shows the relative abundance and mass to charge (m/z) of the di-glycine-modified peptide in cell transfected with non-targeting, control or HUWE1 targeting siRNA.

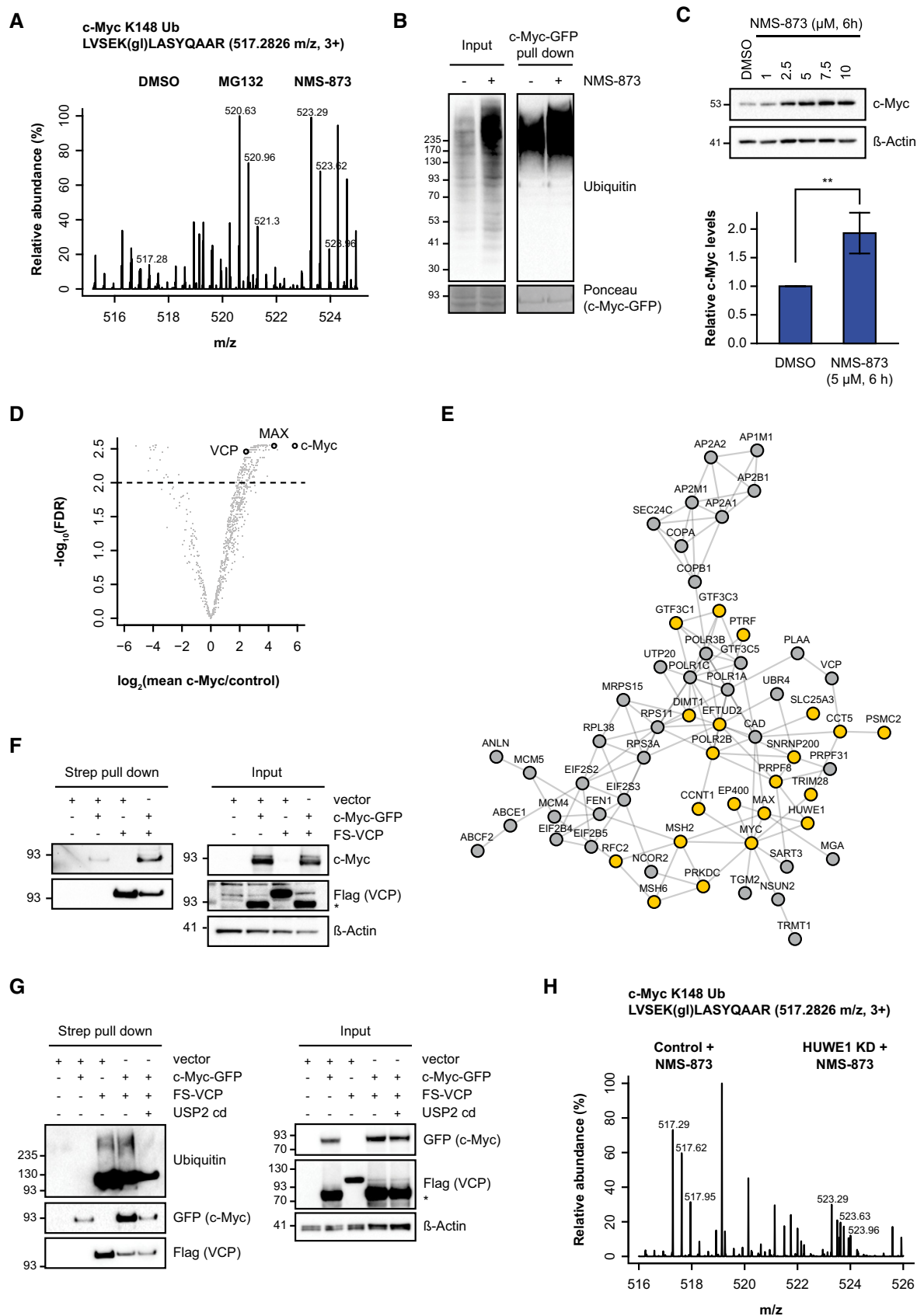


Figure 5.

to bind c-Myc highlighting the complex regulation of this transcription factor in cells (Fig 5E). We validated the interaction between c-Myc and VCP in cells by immunoprecipitation of VCP or c-Myc followed by Western blotting (Figs 5F and EV5H). Treatment of immunoprecipitates with the catalytic domain of USP2 abolished the binding between c-Myc and VCP, indicating that the interaction occurs in an ubiquitin-dependent manner (Fig 5G). Among the identified c-Myc interaction partners was also HUWE1, which has been previously reported to be involved in ubiquitylation and regulation of c-Myc (Fig 5E) [61–63]. Ubiquitin remnant profiling revealed that knockdown of HUWE1 specifically decreased the ubiquitylation of c-Myc on lysine 148 after VCP inhibition, suggesting that HUWE1-dependent ubiquitylation is important for c-Myc binding to VCP (Fig 5H).

In line with the hypothesis that VCP might be required for extraction of c-Myc from the highly structured c-Myc-Max heterodimer and chromatin, and its subsequent degradation through the proteasome, we found that knockdown of VCP resulted in increased association of ubiquitylated c-Myc with chromatin (Fig 6A). In addition, the amount of endogenous Max that co-immunoprecipitated with Myc increased in VCP knockdown cells (Fig 6B).

It has been shown that ubiquitylation and proteasomal turnover of chromatin-associated c-Myc positively regulates its function in gene expression by promoting the assembly of protein complexes involved in transcriptional elongation [64–68]. To investigate the functional consequences of VCP-dependent c-Myc degradation, we monitored the transcriptional activity of c-Myc using the pMyc-TA-Luc luciferase reporter construct. Notably, we found that downregulation of VCP decreased the basal levels of c-Myc transcriptional activity despite the increased cellular levels of c-Myc in these conditions (Fig 6C). The transcriptional activity of ectopically expressed tagged version of c-Myc also decreased after VCP knockdown in agreement with the finding that VCP regulates c-Myc function on the post-translational level (Fig 6C).

We also tested whether VCP regulates the transcription of c-Myc target genes in U2OS cells (Fig EV5I). In line with the observation that VCP depletion decreased c-Myc transcriptional activity, we found that the ability of endogenous c-Myc to promote the

expression of its target genes decreased upon depletion of VCP (Fig 6D). To further study the effects of VCP inhibition on gene expression, we performed RNA sequencing in untreated cells and in cells treated with the VCP inhibitor NMS-873. Chemical inhibition of VCP resulted in significant upregulation of 1,507 and downregulation of 2,594 genes (Dataset EV7). As previously reported for CB-5083, enrichment analysis of genes upregulated after VCP inhibition using NMS-873 revealed genes involved in the unfolded protein response (Fig EV5J). Inhibition of VCP also significantly decreased the transcription of the c-Myc target genes *Skp2*, *Tfap4*, and *E2f2* as observed by RT-PCR after knockdown of VCP. Furthermore, gene set enrichment analysis (GSEA) showed that multiple sets of Myc-induced genes were significantly repressed after VCP inhibition (Fig 6E). Taken together, our data demonstrate that VCP-dependent degradation of ubiquitylated c-Myc on chromatin is important for promoting its function in gene expression (Fig 6F).

Discussion

VCP is an evolutionarily conserved ATPase that plays essential roles in regulating the degradation of cellular proteins through the ubiquitin–proteasome system [7–9,19]. The function of VCP in the degradation of misfolded proteins during ERAD is well established [13,69]. In addition, VCP has been implicated in the remodeling and degradation of specific proteins in other cellular compartments [19]. However, most studies performed so far focused on single VCP substrate proteins leaving the scope of VCP in the cellular protein homeostasis as well as the identity and properties of its substrates largely undefined.

In this study, we combined enrichment of ubiquitin remnant peptides and SILAC-based quantitative MS to monitor changes in the ubiquitin-modified proteome after VCP inhibition and to define the substrate spectrum of VCP in human cells. We identified many previously known as well as ~450 novel putative VCP substrates and provide information about the ubiquitylation sites that respond to VCP inhibition, thereby enabling further focused studies of VCP

Figure 6. VCP regulates the activity of c-Myc in gene expression.

- A VCP inhibition promotes the association of c-Myc with chromatin. Chromatin-associated proteins were extracted from cells with increasing concentrations of salt (100–300 mM NaCl). Individual protein fractions from untreated and VCP inhibitor-treated cells were subjected to Western blotting using the indicated antibodies. Knockdown of c-Myc was used as control to confirm the specificity of the detected bands.
- B c-Myc interaction with endogenous Max is enhanced after VCP knockdown. c-Myc-Flag-Strep was ectopically expressed in U2OS cells and pulled down using StrepTactin Sepharose. Bound proteins were resolved by SDS–PAGE and blotted with the indicated antibodies.
- C VCP promotes c-Myc transcriptional activity. U2OS cells were transfected with VCP siRNA or a non-targeting, control siRNA and c-Myc transcriptional activity was monitored with luciferase-based c-Myc reporter assays in cells expressing endogenous c-Myc and upon c-Myc overexpression. The bar plot shows the mean and SD calculated from three replicate experiments. *** $P < 0.001$, ** $P < 0.01$, * $P < 0.05$ (two-tailed, unpaired, equal variance Student's *t*-test). The Western blot shows the levels of VCP and c-Myc in one of the representative experiments. The line indicates cropped lanes.
- D RT–PCR analysis of c-Myc target genes and VCP in U2OS cells transfected with control, non-targeting siRNA and two VCP siRNA sequences. The bar plot shows the mean and SD calculated from three replicate experiments. *** $P < 0.001$, ** $P < 0.01$, * $P < 0.05$ (two-tailed, unpaired, equal variance Student's *t*-test).
- E c-Myc-induced genes are repressed after chemical VCP inhibition. Total RNA-seq analysis was performed from U2OS cells treated with the VCP inhibitor NMS-873 (5 μ M NMS-873, 4 h) or from mock-treated cells. GSEA analysis of regulated genes in comparison with previously identified sets of MYC-regulated genes (upper panel). Enrichment plots showing the most significant MYC-induced gene sets (lower panel). The complete results of the differential expression analysis after VCP inhibition can be found in Dataset EV7.
- F Schematic representation of the model for c-Myc regulation by VCP. c-Myc binds chromatin at transcription start sites as heterodimer with Max and promotes the transcription of many genes. Ubiquitylation of c-Myc on lysine 148 that is dependent on HUWE1 leads to binding of VCP. Remodeling of c-Myc by VCP might be required for its removal from the highly structured c-Myc/Max heterodimer. VCP-dependent turnover and proteasomal degradation of c-Myc on chromatin promotes its activity in gene expression.

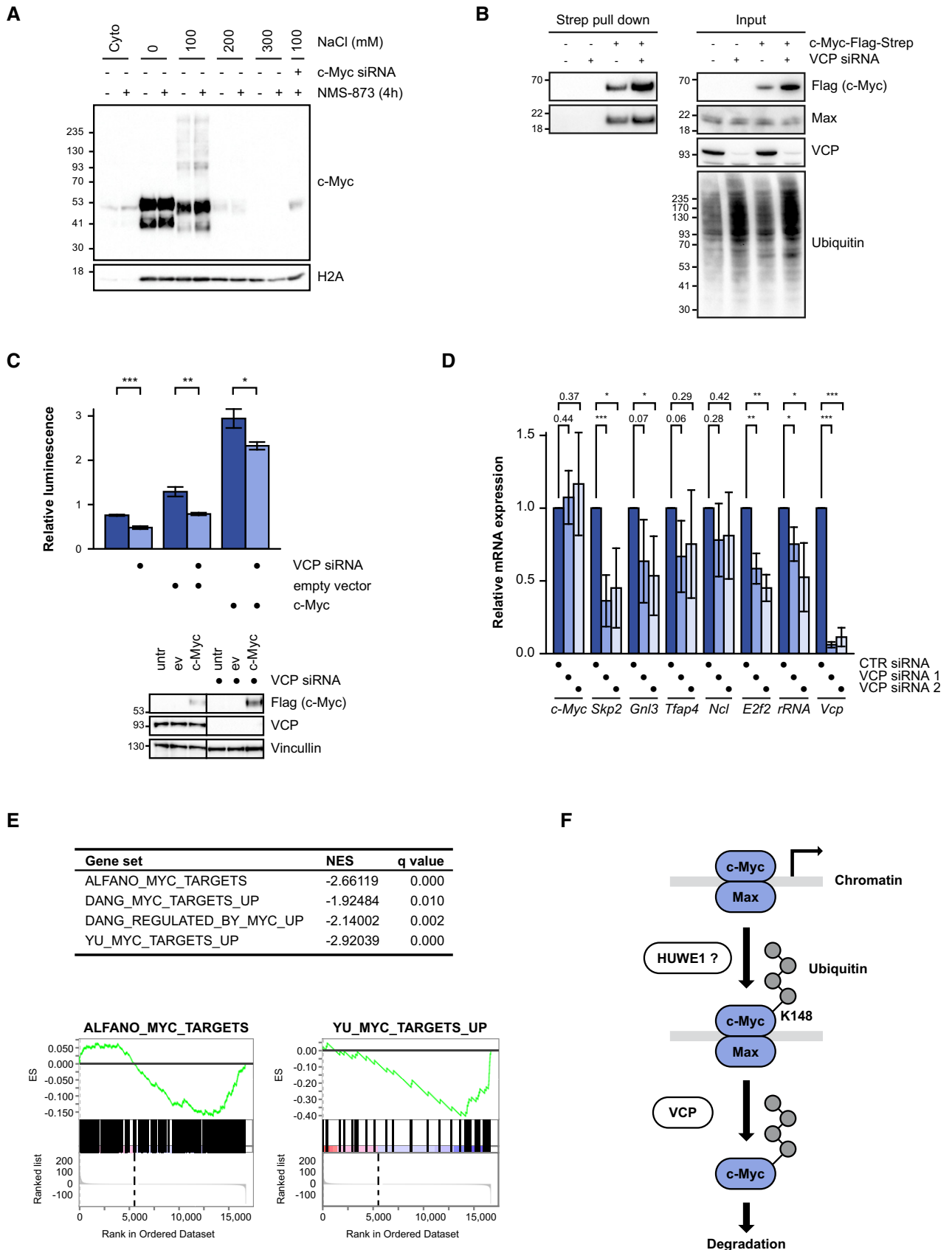


Figure 6.

in different cellular processes. We revealed that VCP substrates are poor in disordered, low complexity regions. It has been previously shown that the proteasome requires unstructured initiation sites in substrate proteins for efficient degradation, and that the degradation of tightly folded proteins is enhanced when an unstructured region is attached to a substrate [70,71]. Our study now provides evidence on a proteome-wide level that the amount of disordered regions is one of the features that determines the requirement of VCP for degradation of proteins by the proteasome in human cells.

We demonstrate that VCP regulates a number of nuclear proteins involved in gene expression, DNA repair, and cell cycle regulation. In addition to nucleotide-excision repair factors, we also identified DNA double strand-break repair proteins including TRIM28/KAP1, BRCC3, and UIMC1/RAP80 as putative VCP substrates. Degradation of cell cycle factors CCNE1, CDC25A, and CDK inhibitor FAR1 has been previously shown to be mediated by VCP or its yeast homologue *cdc48*, respectively [58,72,73]. Our findings indicate that VCP mediates the degradation of additional cell cycle regulators.

Interestingly, one-third of the identified VCP substrates showed increased ubiquitylation only after inhibition of VCP, but not after proteasome inhibition, suggesting that VCP does not mediate proteasomal degradation of these proteins. In human cells, VCP has been shown to extract Aurora B kinase from chromatin without subsequent degradation [20,21]. Our data suggest that the scope of VCP in the proteasome-independent extraction of proteins from cellular structures or protein complexes is broader than previously anticipated and extends to other cellular processes including vesicle-mediated transport and EGFR signaling pathway.

Apart from the identity and nature of proteins regulated by VCP, the types of ubiquitin chains that function in concert with VCP in different cellular processes have not been systematically investigated. It has been shown that K11/K48-branched ubiquitin chains are more efficiently recognized by VCP compared to homotypic K11- or K48-linked chains [41,42]. In support of this, we find that VCP inhibition leads to an upregulation of K11- and K48-linked ubiquitylation in cells. Importantly, we associate K6-linked ubiquitylation with VCP functions and define a network of proteins regulated by this atypically linked ubiquitylation. Little is known about the cellular functions of K6-linked ubiquitylation: K6-linked ubiquitin can be assembled by the ubiquitin ligase parkin and has recently been implicated in the mitochondrial quality control [44–46,74]. We show that the K6-linked ubiquitylation that accumulates in cells after VCP inhibition is assembled by the HECT-type ubiquitin ligase HUWE1. While this work was under review, David Komander and colleagues reported that HUWE1 can assemble K6-linked ubiquitylation and identified mitofusin-2 as a substrate [47]. A recent study that systematically investigated proteins binding to differently linked diubiquitin identified VCP as specific interactor of K6- and K48-linked diubiquitin [75]. Interestingly, the UBA domain of the VCP adaptor UBXN1 was also shown to bind K6-linked ubiquitin [76]. We identified UBXN1 in the K6-linked ubiquitin-specific pull downs and showed that UBXN1 is ubiquitylated by HUWE1. However, it remains to be investigated whether UBXN1 recruits proteins modified with K6-linked ubiquitylation to VCP in cells or if other VCP cofactors and adaptors are involved. HUWE1 and VCP have been recently shown to jointly regulate a

cytosolic protein quality control pathway that degrades unassembled soluble proteins [77]. It is plausible that K6-linked ubiquitylation of proteins mediated by HUWE1 and recognized by VCP is important in this pathway.

The cellular levels and functions of the transcription factor c-Myc are extensively regulated by dynamic ubiquitylation and deubiquitylation that is mediated by a number of ubiquitin ligases and deubiquitylating enzymes [59]. c-Myc binds chromatin only after forming a heterodimer with Max and activates the transcription of many genes [78–80]. It has been previously shown that c-Myc ubiquitylation occurs on multiple lysine residues, and that proteasomal degradation positively regulates c-Myc function in gene expression activation [29,31,59,64]. However, the detailed mechanism underlying c-Myc degradation on chromatin remains unknown. Using affinity purification-MS with c-Myc as bait, we found that c-Myc interacts with VCP. Chemical inhibition or knockdown of VCP results in increased c-Myc ubiquitylation and increased c-Myc protein levels on chromatin. Thus, VCP might be needed to extract c-Myc from the Myc/Max heterodimer before its degradation by the proteasome, which has been reported to be recruited to sites of active transcription [81–86]. In budding yeast, it has been shown that *cdc48* is required for the release of the ubiquitylated transcriptional repressor $\alpha 2$ from chromatin prior to its degradation [87]. We now show that VCP can also remodel and degrade transcription factor c-Myc in human cells. Importantly, VCP-dependent degradation promotes c-Myc function in the activation of gene expression. At least three ubiquitin ligases, FBXO28, HUWE1, and SKP2, have been reported to positively regulate c-Myc function in gene expression [61,64–67]. We show that VCP inhibition leads to increased c-Myc ubiquitylation on its N-terminal lysine (K148) that is dependent on HUWE1. In a c-Myc/Max highly structured heterodimer, K148 is located away from the DNA and is thus readily accessible to other proteins and to the ubiquitylation machinery. We found that ubiquitylation of this site is dependent on HUWE1; however, we never detected c-Myc in K6-linked ubiquitin-specific pull downs, indicating that K148 in c-Myc is predominantly modified with K48-linked ubiquitylation. Interestingly, K148 on c-Myc is also acetylated by the acetyltransferase p300 [88]. It is possible that dynamic modification of this amino acid residue by acetylation and ubiquitylation co-regulates c-Myc interaction with VCP and thereby its function in gene expression regulation.

Taken together, we employed ubiquitin remnant profiling to define the response of the cellular ubiquitylome to VCP inhibition and to identify VCP substrates. We demonstrate that VCP regulates many nuclear and chromatin-associated proteins and promotes the degradation and activity of the transcription factor c-Myc. Furthermore, we show that VCP inhibition increases the cellular abundance of K6-linked ubiquitylation that is dependent on HUWE1, and define the network of proteins that are regulated by this atypical ubiquitylation. Proteasome inhibitors are used in clinics for the treatment of multiple myeloma. The VCP inhibitor CB-5083 is currently explored as an alternative approach to target the UPS in different types of hematological and solid malignancies [25,26]. We find that VCP inhibition increases ubiquitylation of a different subset of proteins compared to proteasome inhibition, thus providing information that might help to understand the clinical effects of these inhibitors.

Material and Methods

Cell culture

Human osteosarcoma cells (U2OS) were obtained from ATCC and cultured in D-MEM medium supplemented with 10% fetal bovine serum, L-glutamine, penicillin, and streptomycin. U2OS ubiquitin replacement cells were generously provided by Wade Harper (Harvard Medical School, Cambridge, MA) and previously described [48]. To induce ubiquitin shRNA expression and expression of shRNA-resistant replacement wild-type and K6R ubiquitin, cells were treated for 4–5 days with 2 µg/ml doxycycline. For SILAC labeling, cells were cultured in media containing either L-arginine and L-lysine, L-arginine [13C6] and L-lysine [2H4], or L-arginine [13C615N4] and L-lysine [13C6-15N2] (Cambridge Isotope Laboratories) as described previously [89]. All cells were cultured at 37°C in a humidified incubator at 5% CO₂.

Transfection of siRNA

Cells were transfected with siRNAs using Lipofectamine RNAiMAX (Life Technologies) according to the manufacturer's instructions.

Cell lysis

Cells were treated with 10 µM MG132 (Sigma), 5 µM NMS-873, or 0.5 µM CB-5083 (Selleckchem) for the indicated periods and subsequently washed with ice-cold phosphate-buffered saline. Cells were lysed in modified RIPA buffer (50 mM Tris pH 7.5, 150 mM NaCl, 1 mM EDTA, 1% NP-40, 0.1% sodium deoxycholate) supplemented with protease inhibitors (Complete protease inhibitor cocktail tablets, Roche Diagnostics), 1 mM sodium orthovanadate, 5 mM β-glycerophosphate, 5 mM sodium fluoride, and 10 mM N-ethylmaleimide (all from Sigma). NaCl was added to a final concentration of 500 mM, and lysates were briefly sonicated to release the chromatin-bound proteins. Subsequently, lysates were cleared by centrifugation at 16,000 × *g* for 15 min and protein concentrations were estimated using QuickStart Bradford Protein assay (Bio-Rad). Cellular fractionation was performed as described previously [90].

MS sample preparation

Proteins were precipitated in fourfold excess of ice-cold acetone and subsequently re-dissolved in denaturation buffer (6 M urea, 2 M thiourea in 10 mM HEPES pH 8.0). Cysteines were reduced with 1 mM dithiothreitol and alkylated with 5.5 mM chloroacetamide [91]. Proteins were digested with endoproteinase Lys-C (Wako Chemicals) and sequencing grade modified trypsin (Sigma). Protease digestion was stopped by addition of trifluoroacetic acid to 0.5%, and precipitates were removed by centrifugation. Peptides were purified using reversed-phase Sep-Pak C18 cartridges (Waters) and eluted in 50% acetonitrile. For ubiquitin remnant peptide enrichment, 20 mg of peptides was re-dissolved in immunoprecipitation buffer (10 mM sodium phosphate, 50 mM sodium chloride in 50 mM MOPS pH 7.2). Precipitates were removed by centrifugation. Modified peptides were enriched using 40 µl of di-glycine-lysine antibody resin (Cell Signaling Technology). Peptides were incubated with the antibodies for 4 h at 4°C on a rotation wheel. The beads were washed three times in ice-

cold immunoprecipitation buffer followed by three washes in water. The enriched peptides were eluted with 0.15% trifluoroacetic acid in H₂O, fractionated in six fractions using micro-column-based strong-cation exchange chromatography (SCX) [92], and desalted on reversed-phase C18 StageTips [93].

For proteome analysis, 20 µg of protein from each SILAC condition (60 µg in total) was pooled and separated by SDS-PAGE. NuPAGE[®] LDS Sample Buffer (Life Technologies) supplemented with 1 mM dithiothreitol was added to the sample. The sample was heated at 70°C for 10 min, alkylated by addition of 5.5 mM chloroacetamide, and loaded onto 4–12% gradient Bis-Tris gels. Proteins were stained using the Colloidal Blue Staining Kit (Life Technologies) and digested in-gel using trypsin. Peptides were extracted from gel and desalted on reversed-phase C18 StageTips [93].

MS analysis

Peptide fractions were analyzed on a quadrupole Orbitrap mass spectrometer (Q Exactive Plus, Thermo Scientific) equipped with a UHPLC system (EASY-nLC 1000, Thermo Scientific) as described [94,95]. Peptide samples were loaded onto C18 reversed-phase columns (15 cm length, 75 µm inner diameter, 1.9 µm bead size) and eluted with a linear gradient from 8 to 40% acetonitrile containing 0.1% formic acid in 2 h. The mass spectrometer was operated in data-dependent mode, automatically switching between MS and MS² acquisition. Survey full scan MS spectra (*m/z* 300–1,700) were acquired in the Orbitrap. The 10 most intense ions were sequentially isolated and fragmented by higher energy C-trap dissociation (HCD) [96]. An ion selection threshold of 5,000 was used. Peptides with unassigned charge states, as well as with charge states < +2, were excluded from fragmentation. Fragment spectra were acquired in the Orbitrap mass analyzer.

Peptide identification

Raw data files were analyzed using MaxQuant (development version 1.5.2.8) [97]. Parent ion and MS² spectra were searched against a database containing 88,473 human protein sequences, human protein sequences obtained from the UniProtKB released in December 2016 using Andromeda search engine [98]. Spectra were searched with a mass tolerance of 6 ppm in MS mode, 20 ppm in HCD MS² mode, strict trypsin specificity and allowing up to three miscleavages. Cysteine carbamidomethylation was searched as a fixed modification, whereas protein N-terminal acetylation, methionine oxidation, N-ethylmaleimide modification of cysteines (mass difference to cysteine carbamidomethylation), and di-glycine-lysine were searched as variable modifications. Site localization probabilities were determined by MaxQuant using the PTM scoring algorithm as described previously [97,99]. The dataset was filtered based on posterior error probability (PEP) to arrive at a false discovery rate of below 1% estimated using a target-decoy approach [100]. Di-glycine lysine-modified peptides with a minimum score of 40 and delta score of 6 are reported and used for the analyses.

Computational analysis

Statistical analysis was performed using the R software environment. Correlation coefficient and significance were determined

using Spearman's rank method. Differences in SILAC ratio variance were assessed using the Siegel–Tukey test. Biophysical protein properties were determined using the ProtParam module from the Biopython project [101]. The GRAVY score is defined by the sum of hydrophathy values of all amino acids divided by the protein length [102]. The fraction of protein sequence containing disordered regions for each protein was determined using MobiDB 2.0 [103]. Statistical significance was calculated using Wilcoxon rank sum test. Functional protein interaction network analysis was performed using interaction data from the STRING database [104]. Only interactions with a score > 0.7 are represented in the networks. Cytoscape version 3.1.1 was used for visualization of protein interaction networks [105]. For GO enrichment analysis, Gene Ontology Annotation was obtained from Uniprot and the significance of the enrichment of a specific term was determined using Fisher's exact test. *P* values were corrected for multiple hypotheses testing using the Benjamini and Hochberg FDR.

Pull-down assays for detection of ubiquitylated proteins

Vectors encoding GFP-tagged proteins or GFP alone were transfected using polyethylenimine in U2OS cells. After 48 h, transfected cells from one 100-mm dish were lysed in 300 μ l of lysis buffer (50 mM Tris–HCl pH 7.5, 150 mM NaCl, 1 mM EDTA, 0.5% Triton X-100, protease inhibitors (Complete protease inhibitor cocktail tablets, Roche Diagnostics), 10 mM N-ethylmaleimide), and lysates were prepared as described above. 20 μ l of pre-equilibrated GFP-Trap_A beads (Chromotek) was added to the cleared lysate and incubated 1 h at 4°C on a rotation wheel. For detection of protein ubiquitylation, washing was performed as follows: The beads were washed once with buffer containing 10 mM Tris–HCl pH 7.5, 150 mM NaCl, 0.5 mM EDTA, protease inhibitors, 10 mM N-ethylmaleimide followed by three washes with 8 M urea, 1% SDS in 1 \times PBS and once with 1% SDS in 1 \times PBS [106]. Bound proteins were eluted in NuPAGE[®] LDS Sample Buffer (Life Technologies) supplemented with 1 mM dithiothreitol, heated at 70°C for 10 min, and loaded onto 4–12% gradient SDS–PAGE gels.

Pull-down assays for analyzing protein interactions

Cells were lysed in lysis buffer (50 mM Tris–HCl pH 7.5, 150 mM NaCl, 1 mM EDTA, 0.5% Triton, protease inhibitors (Complete protease inhibitor cocktail tablets, Roche Diagnostics), 10 mM N-ethylmaleimide), and lysates were prepared as described in “Cell lysis” section. 20 μ l of pre-equilibrated GFP-Trap_A beads (Chromotek) or StrepTactin Sepharose (IBA) was added to the cleared lysate and incubated 1 h in the cold room on a rotation wheel followed by four washes with lysis buffer. In case of USP2 cd digestion, immunoprecipitates were washed twice with lysis buffer, incubated for 15 min with 500 nM USP2 cd on ice, and washed subsequently twice with lysis buffer. For SILAC pull downs, after the third wash, beads from each SILAC condition were pooled. Bound proteins were eluted in NuPAGE[®] LDS Sample Buffer (Life Technologies) supplemented with 1 mM dithiothreitol, heated at 70°C for 10 min and loaded onto 4–12% gradient SDS–PAGE gels. In case of MS analysis, protein samples were alkylated with 5.5 mM CAA and then resolved by SDS–PAGE. Proteins were stained using the Colloidal Blue Staining Kit (Life Technologies) and digested

in-gel using trypsin. Peptides were extracted from gel and desalted on reversed-phase C18 StageTips.

Cycloheximide chase assay

Cells were transfected with the siRNA targeting VCP or a non-targeting control siRNA using Lipofectamine RNAiMAX (Life Technologies) according to the manufacturer's instructions. After 72 h, cells were treated for the indicated time points with 100 μ g/ml of cycloheximide (SIGMA) and then lysed.

Enrichment of K6-linked ubiquitylated proteins

One 150-mm dish was used for each SILAC condition in pull-down experiments. Cells were mock-treated or treated with NMS-873 for 6 h and lysed in 500 μ l of modified RIPA buffer (50 mM Tris–HCl pH 7.5, 150 mM NaCl, 1 mM EDTA, 1% NP-40, 0.1% sodium deoxycholate, protease inhibitors, 10 mM N-ethylmaleimide). Lysates were prepared as described in “Cell lysis” section. Lysates were incubated with 1 μ g of GFP-tagged Anti-diUbiquitin K6-linkage Affimer (Avacta Life Sciences) overnight in the cold room on a rotation wheel (2 mg of protein lysate/condition). Next day, 15 μ l of pre-equilibrated GFP-Trap agarose was added for 1 h. The improved dimerized version of the GFP-tagged K6-linked ubiquitin-specific affimer was used in this study [47]. The beads were washed four times with modified RIPA buffer supplemented with protease inhibitors and 10 mM NEM. After the fourth wash, beads from each SILAC condition were pooled. Bound proteins were eluted in NuPAGE[®] LDS Sample Buffer (Life Technologies) supplemented with 1 mM dithiothreitol, heated at 70°C for 10 min, alkylated by addition of 5.5 mM chloroacetamide for 30 min [91], and loaded onto 4–12% gradient SDS–PAGE gels. Proteins were stained using the Colloidal Blue Staining Kit (Life Technologies) and digested in-gel using trypsin. Peptides were extracted from gel and desalted on reversed-phase C18 StageTips.

SDS–PAGE and Western blotting

Proteins were resolved on 4–12% gradient SDS–PAGE gels (NuPAGE[®] Bis–Tris Precast Gels, Life Technologies) and transferred onto nitrocellulose membranes. Membranes were blocked using 10% skimmed milk solution in PBS supplemented with 0.1% Tween-20. Secondary antibodies coupled to horseradish peroxidase (Jackson ImmunoResearch Laboratories) were used in a 1:5,000 dilution for immunodetection. The detection was performed with SuperSignal West Pico Chemiluminescent Substrate (Thermo Scientific).

Cell cycle analysis

Cells were transfected with VCP targeting or control, non-targeting siRNA. 72 h post-transfection cells were incubated with 10 μ M EdU for 1 h prior to collection and fixed in 4% paraformaldehyde solution. Permeabilization of the cells was performed by incubation in 1% BSA in PBS. Click reaction was performed (Alexa Fluor 647 (Thermo Fisher Scientific), 10 mM (+)-sodium L-ascorbate and 2 mM copper (II) sulfate pentahydrate in PBS) for 1 h. Subsequently, cells were incubated for 20 min with 7-AAD viability staining solution (eBioscience) before analysis by flow cytometry using a BD LSRFortessa SORP.

c-Myc reporter assay

U2OS cells were seeded into six-well plates and transfected with 40 pmol of the indicated siRNA using Lipofectamine RNAiMax (Life Technologies) according to the manufacturer's instructions. After 6 h, the cells were co-transfected with 1 µg of the indicated expression plasmid and 1 µg of the c-Myc reporter construct (Qiagen, CCS-012L). After 72 h, the luciferase activity was assayed using Dual-Glo Luciferase Assay System (Promega) according to the manufacturer's instructions. The measurement was performed on Tecan infinite 200Pro plate reader.

Chromatin extraction assay

Cell were washed twice in ice-cold PBS and then resuspended in Buffer A (10 mM HEPES-KOH pH 7.5, 10 mM KCl, 1.5 mM MgCl₂, 0.34 M sucrose, 10% glycerol, 1× Protease Inhibitor Cocktail (Sigma), 1 mM DTT and 0.1% Triton X-100). After a 15-min incubation on ice, whole cell extract was collected and incubated with DNase for 1 h. Cytoplasmic fraction was collected after centrifugation for 5 min at 1,300 × g. Pellet was washed once with Buffer A, and the nuclei were incubated for 1 h on ice with Buffer B (20 mM HEPES pH 7.5, 3 mM EDTA, 10% glycerol, 125 mM potassium acetate, 1.5 mM MgCl₂, 1 mM DTT, 0.5% NP-40, 1× Protease Inhibitor Cocktail (Sigma), DNase). Lysate was centrifuged high speed for 15 min, and the first chromatin fraction was collected from the supernatant. Pellet was resuspended in buffer containing increasing concentrations of NaCl and incubated for 30 min at 4°C. After each extraction step, the chromatin fraction was collected by high-speed centrifugation.

RT-PCR of c-Myc target genes

RNA extraction was performed using the RNeasy Plus Mini Kit (Qiagen) followed by cDNA synthesis using the QuantiTect Reverse Transcription Kit (Qiagen) according to the manufacturer's instructions. Quantitative real-time PCR was performed on a ViiA 7 Real-Time PCR System (Thermo Fisher Scientific) using PowerUp SYBR Green Master Mix (Thermo Fisher Scientific). Data were normalized to B2M gene.

RNA sequencing

Total RNA extraction was performed using the RNeasy Plus Mini Kit (Qiagen). The extraction was performed according to the manufacturer's protocol followed by an additional purification starting with the gDNA elimination to improve RNA quality. NGS library prep was performed with Illumina's TruSeq stranded mRNA LT Sample Prep Kit following Illumina's standard protocol (Part # 15031047 Rev. E). Libraries were prepared with a starting amount of 1,000 ng and amplified in 10 PCR cycles.

Libraries were profiled in a DNA 1000 chip on a 2100 Bioanalyzer (Agilent technologies) and quantified using the Qubit dsDNA HS Assay Kit in a Qubit 2.0 Fluorometer (Life technologies).

All six samples (three replicates of mock-treated and three replicates of NMS-873 treated cells) were pooled in equimolar ratio and sequenced on 1 NextSeq 500 Midoutput Flowcell, single read for 1 × 159 cycles plus seven cycles for the index read.

Reads were aligned on the *Homo sapiens* genome assembly hg19 (GENCODE release 19) and ERCC (External RNA Control Consortium) reference sequences using STAR (version 2.5.2b, parameters: `-outSJfilterReads Unique -outFilterMismatchNmax 2 -outFilterMultimapNmax 10 -alignIntronMin 21 -sjdbOverhang 158 -clip3pAdapterSeq AGATCGGAAGAG`) [107]. The featureCounts program (version 1.5.1, parameter: `-s 2`) was used to count the number of reads overlapping genes [108]. Differentially expressed genes (DEGs) were determined using DESeq2 (release: 1.16.1) with an FDR cutoff of 1% and ERCC spike-in controls for normalization [109]. The Gene Ontology (GO) and pathway enrichment analysis of DEGs were performed using clusterProfiler (release: 3.4.4) and ReactomePA (release: 1.20.2) packages, respectively [110,111].

The Gene Set Enrichment Analysis (GSEA) was performed with the C2 gene sets from MSigDB (<http://software.broadinstitute.org/gsea/msigdb>). The list of genes was ranked using the sign of the shrunken log₂ fold change multiplied by the inverse of the FDR. The number of permutations was set to 1,000, and significant gene sets ($P < 0.005$) related to MYC were selected.

Immunofluorescence and confocal microscopy

Cell were washed 3× with PBS before fixation using 4% PFA solution in PBS containing Hoechst dye (5 µg/ml) for 15 min. After blocking and permeabilization in 0.2% BSA, 0.1% Triton X-100 in PBS for 15 min, cells were stained with c-Myc antibody (1:100 dilution in 1% BSA) for 1 h. Cells were then incubated with Alexa Fluor 488 goat anti-rabbit IgG (1:1,000 dilution in 1% BSA, Life Technologies) and mounted with fluorescent mounting medium (Dako). Images were acquired with the TCS SP5 confocal microscope (Leica) using a 63× oil objective (NA 1.4), fluorescence excitation with an Argon ion laser (488 nm) and constant imaging and detection settings. Image analysis was done in Fiji [112] with a custom written macro measuring the mean intensity of nuclei with an area of 100–400 µm² in a maximum z-projection.

List of antibodies used in this study

Name	Supplier	Dilution
VCP (7F3)	CST (#2649)	1:1,000
c-Myc (Y69)	Abcam (ab32072)	1:1,000
GFP (B-2)	Santa Cruz Biotechnology (sc-9996)	1:1,000
FLAG M2	SIGMA (F1804)	1:2,000
β-Actin	SIGMA (A2228)	1:10,000
GADD45A (H-165)	Santa Cruz Biotechnology (sc-797)	1:2,000
Ubiquitin (P4D1)	Santa Cruz Biotechnology (sc-8017)	1:1,000
CCND2 (D52F9)	CST (#3741)	1:1,000
MAX (C-17)	Santa Cruz Biotechnology (sc-197)	1:1,000
H2A (L88A6)	CST (#3636)	1:1,000
Vinculin	SIGMA (V9264)	1:10,000
HUWE1	CST (#5695)	1:1,000
HA	Roche Diagnostics (11867423001)	1:5,000

List of RT-PCR primers used in this study

Name	Sequence 5'–3'
Ncl	ACTGACCGGGAACTGGGTC
	TGGCCAGTCCAAGGTAAGT
E2f2	ACAAGCCAACAAGAGGCTG
	TCAGTCCTGTCGGGCACTTC
rRNA	AACGGTGGTGTGCGTCC
	TCTCGTCTCACTCAAACCGCC
c-Myc	TCCTACGTTGCGGTCA
	GCTCGTCACTATCTCCA
B2m	GTGCTCGGCTACTCTCTC
	GTCACCTCAATGTCGGAT
Vcp	TGGAGTCAAAGTGGTGAA
	ATGGCAGGAGCATTCTTCTCA
Skp2	CTGTCTCAAGGGTGATTGC
	TGTACACGAAAAGGGCTGAA
Tfap4	ACGGAGAGAAGCTCAGCAAG
	TGAAGCGCTTGAGCTGTGT
Gnl3	TATCCATGGGGCTTACAAGG
	CTGGACTTCGACAGCAAG

List of siRNA sequences used in this study

Name	Sequence 5'–3'
VCP siRNA 1	GAAUAGAGUUGUUCGGAAU[dT][dT]
VCP siRNA 2	GGAGGUAGAUUUGGAAU[dT][dT]
c-Myc	GGUCAGAGUCUGAUCACC[dT][dT]
CTR siRNA 1	UGGUUACAUGUCGACUAA[dT][dT]
CTR siRNA 2	UGGUUACAUGUUUCUGA[dT][dT]
HUWE1 siRNA	GAGUUUGGAGUUUGUGAAG[dT][dT]

Data availability

The mass spectrometry proteomics data have been deposited to the ProteomeXchange Consortium (<http://proteomecentral.proteomexchange.org>) via the PRIDE partner repository [113] with the dataset identifier PXD003936. The genomics data have been deposited in NCBI's Gene Expression Omnibus (<https://www.ncbi.nlm.nih.gov/geo/>) [114] and are accessible through GEO Series accession number GSE107313.

Expanded View for this article is available online.

Acknowledgements

We thank Anja Freiwald for assistance with mass spectrometry analysis. We thank Alban Ordureau and Wade Harper for generously providing the ubiquitin replacement system cells expressing wild-type and K6R ubiquitin. The support of the IMB Microscopy, Flow Cytometry and Genomics Core Facility

and the use of its NextSeq500 (INST 247/870-1 FUGG) are gratefully acknowledged. PB is supported by the Emmy Noether Program (BE 5342/1-1) and SFB 1177 on selective autophagy from the German Research Foundation, the Marie Curie Career Integration Grant from the European Commission (630763). SAW is supported by the LOEWE Program Ubiquitin Networks (Ub-Net) of the State of Hesse (Germany), the Else Kröner-Fresenius-Stiftung (2015_A124), and the Else Kröner-Forschungskolleg Frankfurt.

Author contributions

PB and SAW designed and supervised the research. JBH, AV, MEB, and SR performed experiments. PB, SAW, and JBH analyzed the data. GP analyzed the RNA-seq data. PB, SAW, and JBH wrote the manuscript. All authors read and commented on the manuscript.

Conflict of interest

The authors declare that they have no conflict of interest.

References

- Dikic I (2017) Proteasomal and autophagic degradation systems. *Annu Rev Biochem* 86: 193–224
- Ciechanover A, Kwon YT (2015) Degradation of misfolded proteins in neurodegenerative diseases: therapeutic targets and strategies. *Exp Mol Med* 47: e147
- Dantuma NP, Bott LC (2014) The ubiquitin-proteasome system in neurodegenerative diseases: precipitating factor, yet part of the solution. *Front Mol Neurosci* 7: 70
- Fessart D, Marza E, Taouji S, Delom F, Chevet E (2013) p97/CDC-48: proteostasis control in tumor cell biology. *Cancer Lett* 337: 26–34
- Haines DS (2010) p97-containing complexes in proliferation control and cancer: emerging culprits or guilt by association? *Genes Cancer* 1: 753–763
- Chapman E, Fry AN, Kang M (2011) The complexities of p97 function in health and disease. *Mol Biosyst* 7: 700–710
- Stolz A, Hilt W, Buchberger A, Wolf DH (2011) Cdc48: a power machine in protein degradation. *Trends Biochem Sci* 36: 515–523
- Ye Y (2006) Diverse functions with a common regulator: ubiquitin takes command of an AAA ATPase. *J Struct Biol* 156: 29–40
- Jentsch S, Rumpf S (2007) Cdc48 (p97): a 'molecular gearbox' in the ubiquitin pathway? *Trends Biochem Sci* 32: 6–11
- van den Boom J, Meyer H (2018) VCP/p97-mediated unfolding as a principle in protein homeostasis and signaling. *Mol Cell* 69: 182–194
- Hänzelmann P, Schindelin H (2017) The interplay of cofactor interactions and post-translational modifications in the regulation of the AAA+ ATPase p97. *Front Mol Biosci* 4: 21
- Schuberth C, Buchberger A (2008) UBX domain proteins: major regulators of the AAA ATPase Cdc48/p97. *Cell Mol Life Sci* 65: 2360–2371
- Wolf DH, Stolz A (2012) The Cdc48 machine in endoplasmic reticulum associated protein degradation. *Biochim Biophys Acta* 1823: 117–124
- Christianson JC, Ye Y (2014) Cleaning up in the endoplasmic reticulum: ubiquitin in charge. *Nat Struct Mol Biol* 21: 325–335
- Papadopoulos C, Kirchner P, Bug M, Grum D, Koerver L, Schulze N, Poehler R, Dressler A, Fengler S, Arhaouy K et al (2017) VCP/p97 cooperates with YOD1, UBXD1 and PLAA to drive clearance of ruptured lysosomes by autophagy. *EMBO J* 36: 135–150

16. Tanaka A, Cleland MM, Xu S, Narendra DP, Suen D-F, Karbowski M, Youle RJ (2010) Proteasome and p97 mediate mitophagy and degradation of mitofusins induced by Parkin. *J Cell Biol* 191: 1367–1380
17. Tresse E, Salomons FA, Vesa J, Bott LC, Kimonis V, Yao T-P, Dantuma NP, Taylor JP (2010) VCP/p97 is essential for maturation of ubiquitin-containing autophagosomes and this function is impaired by mutations that cause IBMPFD. *Autophagy* 6: 217–227
18. Buchan JR, Kolaitis R-M, Taylor JP, Parker R, Aizer A, Brody Y, Ler LW, Sonenberg N, Singer RH, Shav-Tal Y et al (2013) Eukaryotic stress granules are cleared by autophagy and Cdc48/VCP function. *Cell* 153: 1461–1474
19. Meyer H, Bug M, Bremer S (2012) Emerging functions of the VCP/p97 AAA-ATPase in the ubiquitin system. *Nat Cell Biol* 14: 117–123
20. Ramadan K, Bruderer R, Spiga FM, Popp O, Baur T, Gotta M, Meyer HH (2007) Cdc48/p97 promotes reformation of the nucleus by extracting the kinase Aurora B from chromatin. *Nature* 450: 1258–1262
21. Sumara I, Quadroni M, Frei C, Olma MH, Sumara G, Ricci R, Peter M (2007) A Cul3-based E3 ligase removes Aurora B from mitotic chromosomes, regulating mitotic progression and completion of cytokinesis in human cells. *Dev Cell* 12: 887–900
22. Dantuma NP, Hoppe T (2012) Growing sphere of influence: Cdc48/p97 orchestrates ubiquitin-dependent extraction from chromatin. *Trends Cell Biol* 22: 483–491
23. Richardson PG, Barlogie B, Berenson J, Singhal S, Jagannath S, Irwin D, Rajkumar SV, Srkalovic G, Alsina M, Alexanian R et al (2003) A phase 2 study of bortezomib in relapsed, refractory myeloma. *N Engl J Med* 348: 2609–2617
24. Bedford L, Lowe J, Dick LR, Mayer RJ, Brownell JE (2011) Ubiquitin-like protein conjugation and the ubiquitin-proteasome system as drug targets. *Nat Rev Drug Discov* 10: 29–46
25. Deshaies RJ (2014) Proteotoxic crisis, the ubiquitin-proteasome system, and cancer therapy. *BMC Biol* 12: 94
26. Anderson DJ, Le Moigne R, Djakovic S, Kumar B, Rice J, Wong S, Wang J, Yao B, Valle E, Kiss von Soly S et al (2015) Targeting the AAA ATPase p97 as an approach to treat cancer through disruption of protein homeostasis. *Cancer Cell* 28: 653–665
27. Raman M, Sergeev M, Garnaas M, Lydeard JR, Huttlin EL, Goessling W, Shah JV, Harper JW (2015) Systematic proteomics of the VCP-UBXD adaptor network identifies a role for UBXN10 in regulating ciliogenesis. *Nat Cell Biol* 17: 1356–1369
28. Xue L, Blythe EE, Freiburger EC, Mamrosh JL, Hebert AS, Reitsma JM, Hess S, Coon JJ, Deshaies RJ (2016) Valosin-containing protein (VCP)–Adaptor interactions are exceptionally dynamic and subject to differential modulation by a VCP inhibitor. *Mol Cell Proteomics* 15: 2970–2986
29. Kim W, Bennett EJ, Huttlin EL, Guo A, Li J, Possemato A, Sowa ME, Rad R, Rush J, Comb MJ et al (2011) Systematic and quantitative assessment of the ubiquitin-modified proteome. *Mol Cell* 44: 325–340
30. Xu G, Paige JS, Jaffrey SR (2010) Global analysis of lysine ubiquitination by ubiquitin remnant immunoprecipitation. *Nat Biotechnol* 28: 868–873
31. Wagner SA, Beli P, Weinert BT, Nielsen ML, Cox J, Mann M, Choudhary C (2011) A proteome-wide, quantitative survey of *in vivo* ubiquitylation sites reveals widespread regulatory roles. *Mol Cell Proteomics* 10: M111.013284
32. Wójcik C, Yano M, DeMartino GN (2004) RNA interference of valosin-containing protein (VCP/p97) reveals multiple cellular roles linked to ubiquitin/proteasome-dependent proteolysis. *J Cell Sci* 117: 281–292
33. Magnaghi P, D'Alessio R, Valsasina B, Avanzi N, Rizzi S, Asa D, Gasparri F, Cozzi L, Cucchi U, Orrenius C et al (2013) Covalent and allosteric inhibitors of the ATPase VCP/p97 induce cancer cell death. *Nat Chem Biol* 9: 548–556
34. Higgins R, Gendron JM, Rising L, Mak R, Webb K, Kaiser SE, Zuzow N, Riviere P, Yang B, Fenech E et al (2015) The unfolded protein response triggers site-specific regulatory ubiquitylation of 40S ribosomal proteins. *Mol Cell* 59: 35–49
35. Larance M, Ahmad Y, Kirkwood KJ, Ly T, Lamond AI (2013) Global subcellular characterization of protein degradation using quantitative proteomics. *Mol Cell Proteomics* 12: 638–650
36. Dantuma NP, Groothuis TAM, Salomons FA, Neeffjes J (2006) A dynamic ubiquitin equilibrium couples proteasomal activity to chromatin remodeling. *J Cell Biol* 173: 19–26
37. Alexandru G, Graumann J, Smith GT, Kolawa NJ, Fang R, Deshaies RJ (2008) UBXD7 binds multiple ubiquitin ligases and implicates p97 in HIF1 α turnover. *Cell* 134: 804–816
38. Zhang Z, Wang Y, Li C, Shi Z, Hao Q, Wang W, Song X, Zhao Y, Jiao S, Zhou Z (2015) The transitional endoplasmic reticulum ATPase p97 regulates the alternative nuclear factor NF- κ B signaling via partial degradation of the NF- κ B subunit p100. *J Biol Chem* 290: 19558–19568
39. Zhang Z, Lv X, Yin W, Zhang X, Feng J, Wu W, Hui C, Zhang L, Zhao Y (2013) Ter94 ATPase complex targets k11-linked ubiquitinated ci to proteasomes for partial degradation. *Dev Cell* 25: 636–644
40. Xu P, Duong DM, Seyfried NT, Cheng D, Xie Y, Robert J, Rush J, Hochstrasser M, Finley D, Peng J (2009) Quantitative proteomics reveals the function of unconventional ubiquitin chains in proteasomal degradation. *Cell* 137: 133–145
41. Meyer H-J, Rape M (2014) Enhanced protein degradation by branched ubiquitin chains. *Cell* 157: 910–921
42. Yau RG, Doerner K, Castellanos ER, Haakonsen DL, Werner A, Wang N, Yang XW, Martinez-Martin N, Matsumoto ML, Dixit VM et al (2017) Assembly and function of heterotypic ubiquitin chains in cell-cycle and protein quality control. *Cell* 171: 918–933
43. Blythe EE, Olson KC, Chau V, Deshaies RJ (2017) Ubiquitin- and ATP-dependent unfoldase activity of P97/VCP•NPLC4•UFD1L is enhanced by a mutation that causes multisystem proteinopathy. *Proc Natl Acad Sci* 114: E4380–E4388
44. Durcan TM, Tang MY, Pérusse JR, Dashti EA, Aguilera MA, McLelland G-L, Gros P, Shaler TA, Faubert D, Coulombe B et al (2014) USP8 regulates mitophagy by removing K6-linked ubiquitin conjugates from parkin. *EMBO J* 33: 2473–2491
45. Cunningham CN, Baughman JM, Phu L, Tea JS, Yu C, Coons M, Kirkpatrick DS, Bingol B, Corn JE (2015) USP30 and parkin homeostatically regulate atypical ubiquitin chains on mitochondria. *Nat Cell Biol* 17: 160–169
46. Ordureau A, Heo J-M, Duda DM, Paulo JA, Olszewski JL, Yanishevski D, Rinehart J, Schulman BA, Harper JW (2015) Defining roles of PARKIN and ubiquitin phosphorylation by PINK1 in mitochondrial quality control using a ubiquitin replacement strategy. *Proc Natl Acad Sci* 112: 201506593
47. Michel MA, Swatek KN, Hospenthal MK, Komander D (2017) Ubiquitin linkage-specific affimers reveal insights into K6-linked ubiquitin signaling. *Mol Cell* 68: 233–246
48. Ordureau A, Heo J-M, Duda DM, Paulo JA, Olszewski JL, Yanishevski D, Rinehart J, Schulman BA, Harper JW (2015) Defining roles of PARKIN and ubiquitin phosphorylation by PINK1 in mitochondrial quality

- control using a ubiquitin replacement strategy. *Proc Natl Acad Sci USA* 112: 6637–6642
49. Smyth GK (2004) Linear models and empirical bayes methods for assessing differential expression in microarray experiments. *Stat Appl Genet Mol Biol* 3: Article 3
 50. Maric M, Maculins T, De Piccoli G, Labib K (2014) Cdc48 and a ubiquitin ligase drive disassembly of the CMG helicase at the end of DNA replication. *Science* 346: 1253596
 51. Moreno SP, Bailey R, Campion N, Herron S, Gambus A (2014) Polyubiquitylation drives replisome disassembly at the termination of DNA replication. *Science* 346: 477–481
 52. Puumalainen MR, Lessel D, Ruthemann P, Kaczmarek N, Bachmann K, Ramadan K, Naegeli H (2014) Chromatin retention of DNA damage sensors DDB2 and XPC through loss of p97 segregase causes genotoxicity. *Nat Commun* 5: 3695
 53. He J, Zhu Q, Wani G, Sharma N, Han C, Qian J, Pentz K, Wang Q, Wani AA (2014) Ubiquitin-specific protease 7 regulates nucleotide excision repair through deubiquitinating XPC protein and preventing XPC protein from undergoing ultraviolet light-induced and VCP/p97 protein-regulated proteolysis. *J Biol Chem* 289: 27278–27289
 54. He J, Zhu Q, Wani G, Wani AA (2017) UV-induced proteolysis of RNA polymerase II is mediated by VCP/p97 segregase and timely orchestration by Cockayne syndrome B protein. *Oncotarget* 8: 11004–11019
 55. Verma R, Oania R, Fang R, Smith GT, Deshaies RJ (2011) Cdc48/p97 mediates UV-dependent turnover of RNA Pol II. *Mol Cell* 41: 82–92
 56. Fullbright G, Rycenga HB, Gruber JD, Long DT (2016) p97 promotes a conserved mechanism of helicase unloading during DNA cross-link repair. *Mol Cell Biol* 36: 2983–2994
 57. Bastola P, Neums L, Schoenen FJ, Chien J (2016) VCP inhibitors induce endoplasmic reticulum stress, cause cell cycle arrest, trigger caspase-mediated cell death and synergistically kill ovarian cancer cells in combination with Salubrinal. *Mol Oncol* 10: 1559–1574
 58. Riemer A, Dobrynin G, Dressler A, Bremer S, Soni A, Iliakis G, Meyer H (2014) The p97-Ufd1-Npl4 ATPase complex ensures robustness of the G2/M checkpoint by facilitating CDC25A degradation. *Cell Cycle* 13: 919–927
 59. Farrell AS, Sears RC (2014) MYC degradation. *Cold Spring Harb Perspect Med* 4: a014365
 60. Amati B, Dalton S, Brooks MW, Littlewood TD, Evan GI, Land H (1992) Transcriptional activation by the human c-Myc oncoprotein in yeast requires interaction with Max. *Nature* 359: 423–426
 61. Adhikary S, Marinoni F, Hock A, Hulleman E, Popov N, Beier R, Bernard S, Quarto M, Capra M, Goettig S et al (2005) The ubiquitin ligase HectH9 regulates transcriptional activation by Myc and is essential for tumor cell proliferation. *Cell* 123: 409–421
 62. Inoue S, Hao Z, Elia AJ, Cescon D, Zhou L, Silvester J, Snow B, Harris IS, Sasaki M, Li WY et al (2013) Mule/Huwe1/Arf-BP1 suppresses Ras-driven tumorigenesis by preventing c-Myc/Miz1-mediated down-regulation of p21 and p15. *Genes Dev* 27: 1101–1114
 63. Zhao X, Heng JI-T, Guardavaccaro D, Jiang R, Pagano M, Guillemot F, Iavarone A, Lasorella A (2008) The HECT-domain ubiquitin ligase Huwe1 controls neural differentiation and proliferation by destabilizing the N-Myc oncoprotein. *Nat Cell Biol* 10: 643–653
 64. Jaenicke LA, von Eyss B, Carstensen A, Wolf E, Xu W, Greifenberg AK, Geyer M, Eilers M, Popov N, Bouchard C et al (2016) Ubiquitin-dependent turnover of MYC antagonizes MYC/PAF1C Complex Accumulation to Drive Transcriptional Elongation. *Mol Cell* 61: 54–67
 65. Cepeda D, Ng H-F, Sharifi HR, Mahmoudi S, Cerrato VS, Fredlund E, Magnusson K, Nilsson H, Malyukova A, Rantala J et al (2013) CDK-mediated activation of the SCF^{FBXO 28} ubiquitin ligase promotes MYC-driven transcription and tumorigenesis and predicts poor survival in breast cancer. *EMBO Mol Med* 5: 1067–1086
 66. von der Lehr N, Johansson S, Wu S, Bahram F, Castell A, Cetinkaya C, Hydrbring P, Weidung I, Nakayama K, Nakayama KI et al (2003) The F-Box Protein Skp2 Participates in c-Myc Proteasomal Degradation and Acts as a Cofactor for c-Myc-Regulated Transcription. *Mol Cell* 11: 1189–1200
 67. Kim SY, Herbst A, Tworkowski KA, Salghetti SE, Tansey WP (2003) Skp2 regulates Myc protein stability and activity. *Mol Cell* 11: 1177–1188
 68. Geng F, Wenzel S, Tansey WP (2012) Ubiquitin and proteasomes in transcription. *Annu Rev Biochem* 81: 177–201
 69. Ye Y, Meyer HH, Rapoport TA (2001) The AAA ATPase Cdc48/p97 and its partners transport proteins from the ER into the cytosol. *Nature* 414: 652–656
 70. Prakash S, Tian L, Ratliff KS, Lehotzky RE, Matouschek A (2004) An unstructured initiation site is required for efficient proteasome-mediated degradation. *Nat Struct Mol Biol* 11: 830–837
 71. Gödderz D, Heinen C, Marchese FP, Kurz T, Acs K, Dantuma NP (2015) Cdc48-independent proteasomal degradation coincides with a reduced need for ubiquitylation. *Sci Rep* 5: 7615
 72. Dai RM, Li CC (2001) Valosin-containing protein is a multi-ubiquitin chain-targeting factor required in ubiquitin-proteasome degradation. *Nat Cell Biol* 3: 740–744
 73. Fu X, Ng C, Feng D, Liang C (2003) Cdc48p is required for the cell cycle commitment point at Start via degradation of the G1-CDK inhibitor Far1p. *J Cell Biol* 163: 21–26
 74. Gersch M, Gladkova C, Schubert AF, Michel MA, Maslen S, Komander D (2017) Mechanism and regulation of the Lys6-selective deubiquitinase USP30. *Nat Struct Mol Biol* 24: 920–930
 75. Zhang X, Smits AH, van Tilburg GBA, Jansen PWTC, Makowski MM, Ovaas H, Vermeulen M (2017) An Interaction Landscape of Ubiquitin Signaling. *Mol Cell* 65: 941–955
 76. Wu-Baer F, Ludwig T, Baer R (2010) The UBXN1 protein associates with autoubiquitinated forms of the BRCA1 tumor suppressor and inhibits its enzymatic function. *Mol Cell Biol* 30: 2787–2798
 77. Xu Y, Anderson DE, Ye Y (2016) The HECT domain ubiquitin ligase HUWE1 targets unassembled soluble proteins for degradation. *Cell Discov* 2: 16040
 78. Lin CY, Lovén J, Rahl PB, Paranal RM, Burge CB, Bradner JE, Lee TI, Young RA (2012) Transcriptional amplification in tumor cells with elevated c-Myc. *Cell* 151: 56–67
 79. Nie Z, Hu G, Wei G, Cui K, Yamane A, Resch W, Wang R, Green DR, Tessarollo L, Casellas R et al (2012) c-Myc is a universal amplifier of expressed genes in lymphocytes and embryonic stem cells. *Cell* 151: 68–79
 80. Kress TR, Sabò A, Amati B (2015) MYC: connecting selective transcriptional control to global RNA production. *Nat Rev Cancer* 15: 593–607
 81. Gonzalez F, Delahodde A, Kodadek T, Johnston SA (2002) Recruitment of a 19S proteasome subcomplex to an activated promoter. *Science* 296: 548–550
 82. Malik S, Shukla A, Sen P, Bhaumik SR (2009) The 19 S proteasome subcomplex establishes a specific protein interaction network at the promoter for stimulated transcriptional initiation *in vivo*. *J Biol Chem* 284: 35714–35724

83. Ezhkova E, Tansey WP (2004) Proteasomal ATPases link ubiquitylation of histone H2B to methylation of histone H3. *Mol Cell* 13: 435–442
84. Auld KL, Brown CR, Casolari JM, Komili S, Silver PA (2006) Genomic association of the proteasome demonstrates overlapping gene regulatory activity with transcription factor substrates. *Mol Cell* 21: 861–871
85. Szutorisz H, Georgiou A, Tora L, Dillon N (2006) The proteasome restricts permissive transcription at tissue-specific gene loci in embryonic stem cells. *Cell* 127: 1375–1388
86. Morris MC, Kaiser P, Rudyak S, Baskerville C, Watson MH, Reed SI (2003) Cks1-dependent proteasome recruitment and activation of CDC20 transcription in budding yeast. *Nature* 423: 1009–1013
87. Wilcox AJ, Laney JD (2009) A ubiquitin-selective AAA-ATPase mediates transcriptional switching by remodelling a repressor-promoter DNA complex. *Nat Cell Biol* 11: 1481–1486
88. Faiola F, Liu X, Lo S, Pan S, Zhang K, Lyman E, Farina A, Martinez E (2005) Dual regulation of c-Myc by p300 via acetylation-dependent control of Myc protein turnover and coactivation of Myc-induced transcription. *Mol Cell Biol* 25: 10220–10234
89. Ong S-E, Blagoev B, Kratchmarova I, Kristensen DB, Steen H, Pandey A, Mann M (2002) Stable isotope labeling by amino acids in cell culture, SILAC, as a simple and accurate approach to expression proteomics. *Mol Cell Proteomics* 1: 376–386
90. Méndez J, Stillman B (2000) Chromatin association of human origin recognition complex, cdc6, and minichromosome maintenance proteins during the cell cycle: assembly of prereplication complexes in late mitosis. *Mol Cell Biol* 20: 8602–8612
91. Nielsen ML, Vermeulen M, Bonaldi T, Cox J, Moroder L, Mann M (2008) Iodoacetamide-induced artifact mimics ubiquitination in mass spectrometry. *Nat Methods* 5: 459–460
92. Weinert BT, Scholz C, Wagner SA, Iesmantavicius V, Su D, Daniel JA, Choudhary C (2013) Lysine succinylation is a frequently occurring modification in prokaryotes and eukaryotes and extensively overlaps with acetylation. *Cell Rep* 4: 842–851
93. Rappsilber J, Mann M, Ishihama Y (2007) Protocol for micro-purification, enrichment, pre-fractionation and storage of peptides for proteomics using StageTips. *Nat Protoc* 2: 1896–1906
94. Michalski A, Damoc E, Hauschild JP, Lange O, Wiegand A, Makarov A, Nagaraj N, Cox J, Mann M, Horning S (2011) Mass spectrometry-based proteomics using Q Exactive, a high-performance benchtop quadrupole Orbitrap mass spectrometer. *Mol Cell Proteomics* 10: M111.011015
95. Kelstrup CD, Young C, Lavalley R, Nielsen ML, Olsen JV (2012) Optimized fast and sensitive acquisition methods for shotgun proteomics on a quadrupole orbitrap mass spectrometer. *J Proteome Res* 11: 3487–3497
96. Olsen JV, Macek B, Lange O, Makarov A, Horning S, Mann M (2007) Higher-energy C-trap dissociation for peptide modification analysis. *Nat Methods* 4: 709–712
97. Cox J, Mann M (2008) MaxQuant enables high peptide identification rates, individualized p.p.b.-range mass accuracies and proteome-wide protein quantification. *Nat Biotechnol* 26: 1367–1372
98. Cox J, Neuhauser N, Michalski A, Scheltema RA, Olsen JV, Mann M (2011) Andromeda: a peptide search engine integrated into the MaxQuant environment. *J Proteome Res* 10: 1794–1805
99. Olsen JV, Blagoev B, Gnäd F, Macek B, Kumar C, Mortensen P, Mann M (2006) Global, *in vivo*, and site-specific phosphorylation dynamics in signaling networks. *Cell* 127: 635–648
100. Elias JE, Gygi SP (2007) Target-decoy search strategy for increased confidence in large-scale protein identifications by mass spectrometry. *Nat Methods* 4: 207–214
101. Cock PJA, Antao T, Chang JT, Chapman BA, Cox CJ, Dalke A, Friedberg I, Hamelryck T, Kauff F, Wilczynski B *et al* (2009) Biopython: freely available Python tools for computational molecular biology and bioinformatics. *Bioinformatics* 25: 1422–1423
102. Kyte J, Doolittle RF (1982) A simple method for displaying the hydropathic character of a protein. *J Mol Biol* 157: 105–132
103. Potenza E, Domenico TD, Walsh I, Tosatto SCE (2015) MobiDB 2.0: an improved database of intrinsically disordered and mobile proteins. *Nucleic Acids Res* 43: D315–D320
104. Franceschini A, Szklarczyk D, Frankild S, Kuhn M, Simonovic M, Roth A, Lin J, Minguez P, Bork P, Von Mering C *et al* (2013) STRING v9.1: protein-protein interaction networks, with increased coverage and integration. *Nucleic Acids Res* 41: D808–D815
105. Saito R, Smoot ME, Ono K, Ruscheinski J, Wang PL, Lotia S, Pico AR, Bader GD, Ideker T (2012) A travel guide to Cytoscape plugins. *Nat Methods* 9: 1069–1076
106. Lee SY, Ramirez J, Franco M, Lectez B, Gonzalez M, Barrio R, Mayor U (2014) Ube3a, the E3 ubiquitin ligase causing Angelman syndrome and linked to autism, regulates protein homeostasis through the proteasomal shuttle Rpn10. *Cell Mol Life Sci* 71: 2747–2758
107. Dobin A, Davis CA, Schlesinger F, Drenkow J, Zaleski C, Jha S, Batut P, Chaisson M, Gingeras TR (2013) STAR: ultrafast universal RNA-seq aligner. *Bioinformatics* 29: 15–21
108. Liao Y, Smyth GK, Shi W (2013) The Subread aligner: fast, accurate and scalable read mapping by seed-and-vote. *Nucleic Acids Res* 41: e108
109. Love MI, Huber W, Anders S (2014) Moderated estimation of fold change and dispersion for RNA-seq data with DESeq2. *Genome Biol* 15: 550
110. Yu G, Wang L-G, Han Y, He Q-Y (2012) clusterProfiler: an R package for comparing biological themes among gene clusters. *OMICS* 16: 284–287
111. Yu G, He Q-Y (2016) ReactomePA: an R/Bioconductor package for reactome pathway analysis and visualization. *Mol Biosyst* 12: 477–479
112. Schindelin J, Arganda-Carreras I, Frise E, Kaynig V, Longair M, Pietzsch T, Preibisch S, Rueden C, Saalfeld S, Schmid B *et al* (2012) Fiji: an open-source platform for biological-image analysis. *Nat Methods* 9: 676–682
113. Vizcaino JA, Deutsch EW, Wang R, Csordas A, Reisinger F, Ríos D, Dianes JA, Sun Z, Farrar T, Bandeira N *et al* (2014) ProteomeXchange provides globally coordinated proteomics data submission and dissemination. *Nat Biotechnol* 32: 223–226
114. Barrett T, Wilhite SE, Ledoux P, Evangelista C, Kim IF, Tomashevsky M, Marshall KA, Phillippy KH, Sherman PM, Holko M *et al* (2013) NCBI GEO: archive for functional genomics data sets—update. *Nucleic Acids Res* 41: D991–D995